Journal of Hazardous Materials, 30 (1992) 151–194
Elsevier Science Publishers B.V., Amsterdam

Effects of obstacles on the spread of a heavy gas—Wind tunnel simulations

K.C. Heidorn, M.C. Murphy* and P.A. Irwin

Rowan Williams Davies & Irwin Inc., 650 Woodlawn Rd. West, Guelph, Ontario, N1K 1B8 (Canada)

and

H. Sahota, P.K. Misra and R. Bloxam

Air Resources Branch, Ontario Ministry of the Environment, 125 Resources Rd., Rexdale, Ontario, M9W 5L1 (Canada)

(Received November 27, 1990; accepted in revised form November 7, 1991)

Abstract

The spread of a heavy gas cloud in terrain with obstacles has been studied in the wind tunnel. Observations were made at scales of 1:100 and 1:50 using video and photographic techniques; concentration measurements were obtained with a high frequency flame ionization detector. Several different obstacle configurations were examined. The results of flow visualization experiments in still air have been used to mathematically describe the spread rate using a box model approach. The addition of a term to the standard box model equation which accounted for the effects of block coverage fit the observations very well. It is argued that the major effect of the obstacles is to reduce the rate at which the hydrostatic pressure head declines and increases the path length over which the cloud must move rather than retarding the flow through friction or drag.

1. Introduction

Many of the field studies of dispersion of heavier-than-air gases have been performed in smooth terrain with obstacles which were much smaller than the height of the gas cloud. Historically, however, accidental releases of heavy gases have occurred in or near urban centers where the obstacle sizes (e.g., buildings) have not been small compared with the height of the cloud. The purpose of the work described herein was to study the flow behaviour and concentration

Correspondence to: Dr. K.C. Heidorn, Rowan Williams Davies & Irwin Inc., 650 Woodlawn Rd. West, Guelph, Ontario, N1K 1B8 (Canada).
*Current affiliation: New Brunswick Department of the Environment, P.O. Box 6000, Fredericton, New Brunswick E3B 5H1 (Canada).

0304-3894/92/$03.50

history of an instantaneous release of a heavier-than-air gas in an area where large obstacles would affect the dispersion of the cloud [1].

This paper describes the results of several experiments conducted in the wind tunnel at model scales of 1:100 and 1:50. During a typical experiment, a cylindrical canister was filled with gas at a density determined by Richardson number scaling. The movement of the heavy gas cloud was recorded on video tape during tests where the cloud was marked with smoke. In other tests, the cloud was marked with propane and the concentration was measured with a high frequency flame ionization detector (FID). For detailed procedures and results of this experiment, the reader is referred to [1].

This paper also describes the results of several of the flow visualization experiments of heavy gas releases under still-air conditions (i.e. no wind) for a variety of block configurations. These flow visualization experiments were then used to alter the mathematical box model for the spread rate of the heavy gas cloud to account for flow through large obstacles (i.e., obstacles larger than cloud height).

2. Summary of scaling parameters

In general, physical modelling consists of simulating the physical processes of gas dispersion at full scale by reproducing the approach wind flow and its interaction with a spilled gas. Ideally, the release is scaled by a characteristic length dimension and time scale. The radius or height of the release are often used as the appropriate length scale. The important scaling parameters in heavy gas dispersion are: the Reynolds number of the approach flow $Re = LU\rho/\mu$; the density ratio of the release gas to ambient air ρ_g/ρ_a; and the bulk Richardson number $Ri = gL\,[(\rho_g - \rho_a)/\rho_a]/U^2$, based on the density ratio and the windspeed (U) at 10 m height [2]. The most important are Ri and the density ratio. The Richardson number is used to scale the tunnel velocity for non-zero ambient flows. Higher gas densities allow higher wind tunnel velocities. Since operation of a wind tunnel with speeds less than 1 m/s may produce non-uniform flows, Richardson number scaling is used to set the minimum density required to maintain uniform flow in the tunnel. In the cases of still air or calm ambient wind speeds, the velocity of the heavy gas cloud as calculated by eq. (3) below is used as the characteristic velocity in scaling. Accurate velocity and turbulence measurements are required at these low wind tunnel speeds to ensure that arrival times and concentrations are correct [3–7].

The appropriate time scales may be obtained for releases under calm winds (zero windspeeds) from:

$$t_0 = r_0/U_0 \tag{1}$$

and

$$(r_0/U_0)_{\text{model}} = (r_0/U_0)_{\text{full scale}}, \tag{2}$$

where

$$U_0 = [gh_0(\rho_g - \rho_a)/\rho_a]^{1/2} \tag{3}$$

and r_0, h_0 are the initial radius and height of the release respectively [8]. With non-zero wind conditions, the following scaling is used. By maintaining the following:

$$(Ut/L)_{\text{full scale}} = (Ut/L)_{\text{model}}, \tag{4}$$

the full-scale time can be derived as

$$t_{\text{full scale}} = t_{\text{model}}[U_{\text{model}}/U_{\text{full scale}})\ (L_{\text{full scale}}/L_{\text{model}})]. \tag{5}$$

These equations are useful when converting the actual timing measured in the wind tunnel for comparison with data measured in the field.

3. Experimental procedure

3.1 Wind tunnel simulation of atmospheric wind flows

The simulated heavy gas releases under non-zero winds were conducted in the RWDI boundary-layer wind tunnel (Fig. 1). The simulations were patterned after the heavy gas releases at Thorney Island with emphasis on Heavy Gas Dispersion Trial (HGDT) # 13 [8]. The parameters of this release are given in Table 1. Based on Richardson number scaling (i.e. keeping the *Ri* at model scale equal to the *Ri* at full scale), the required wind speed at various model scales was computed for several different densities. The operation of the wind tunnel at velocities less than 1 m/s produced non-uniform velocity profiles in the cross-tunnel direction. With this in mind and the practical gas densities available, the model scales of 1:50 and 1:100 were chosen for the simulations.

The wind tunnel simulation of the instantaneous releases at Thorney Island required an appropriate design for the holding tank and the release mechanism. For an instantaneous release of heavy gas, a cylindrical release canister (Fig. 2a) was used with a fixed top cover. The gas mixture was pumped into the bottom of the container until the canister was full. The canister cylinder was dropped shortly after filling was completed to prevent significant density stratification of gas in the canister. To initiate the release, two solenoids were activated which allowed the canister cylinder to fall away from the top cover and through the floor of the test platform. Fig. 2(b) shows the release canister

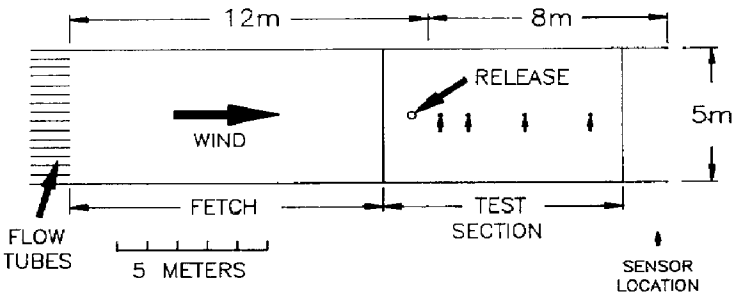

Fig. 1. Plan view of RWDI wind tunnel #2.

and resulting cloud behaviour during one of the experimental trials. The 1:50 release canister and the 1:100 release canister were constructed with the dimensions presented in Table 2. For detailed canister specifications and release mechanisms, the reader is referred to [1].

The still-air experiments were performed on a circular platform with center release point in a room where air motions were at a minimum. Although releases from both 1:50 and 1:100 scale release canisters were made, only results from the 1:50 scale releases were used in the cloud spread study. In experi-

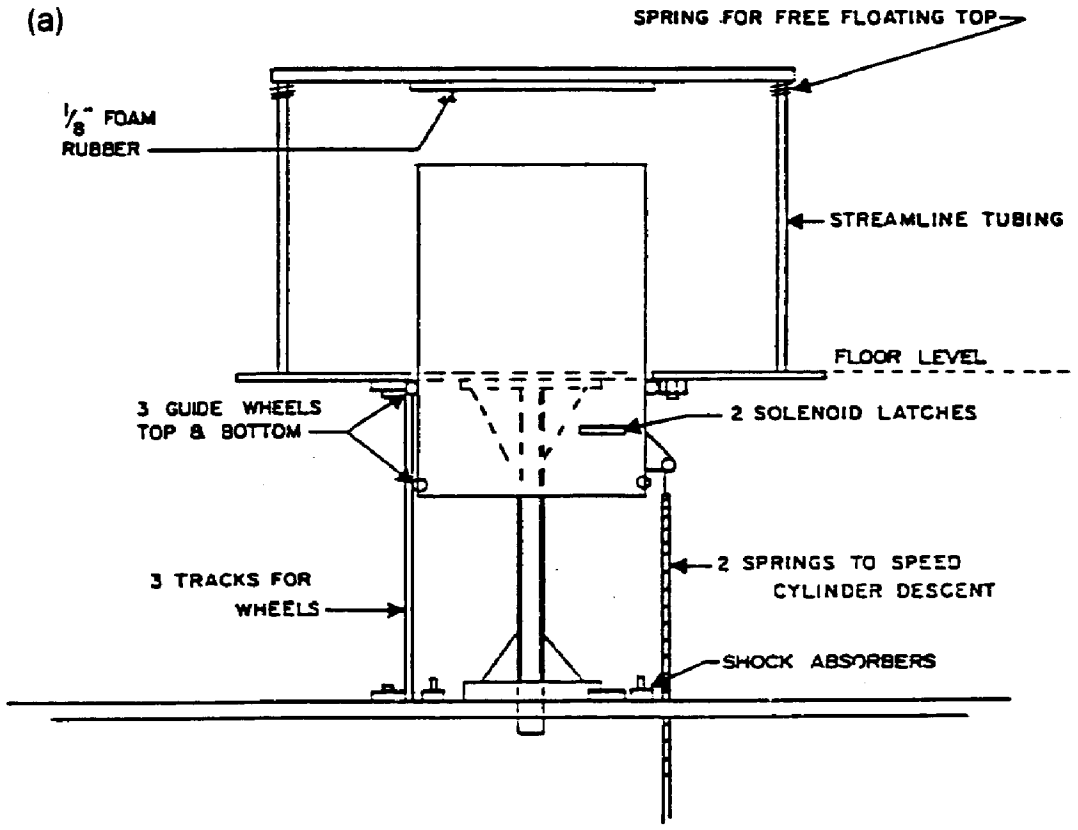

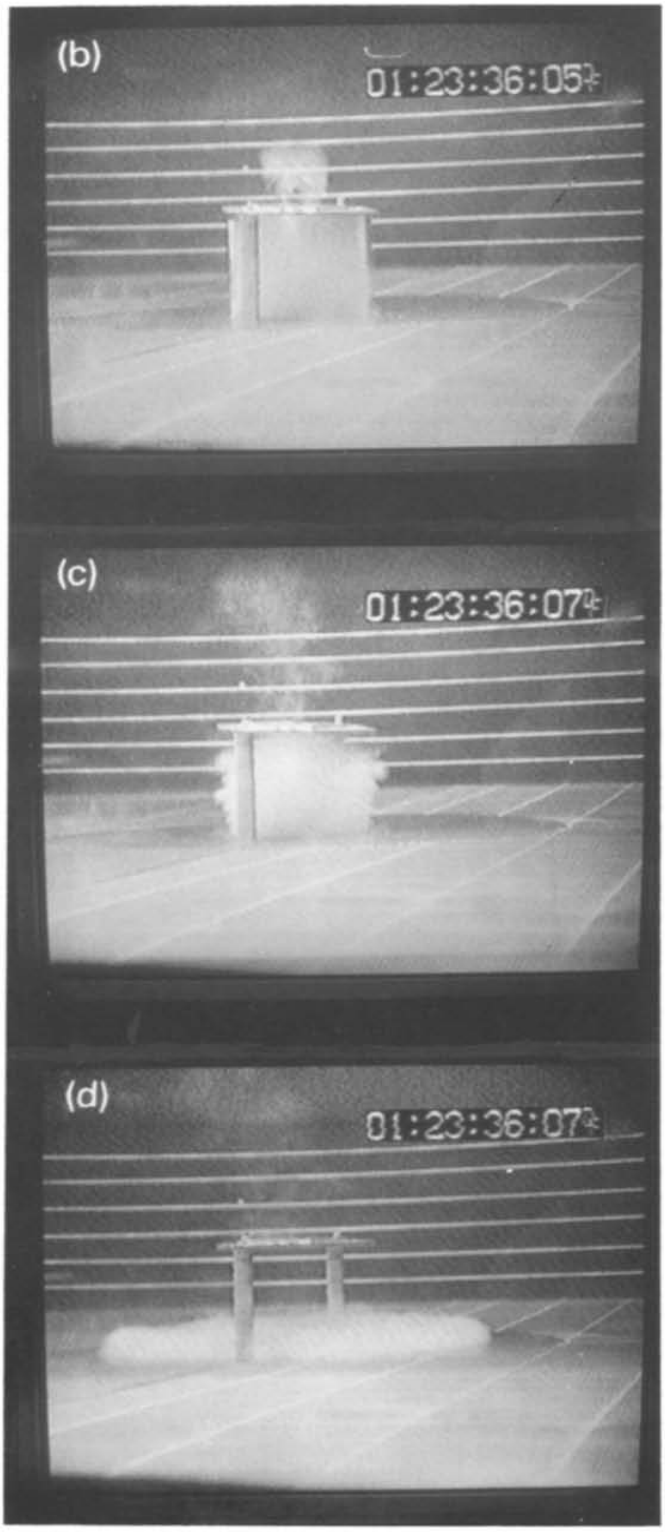

Fig. 2. Heavy gas canister release mechanism. (a) Schematic of canister release mechanism; (b) gas position after canister wall has dropped through floor; (c) gas cloud 1/15 s later, and (d) gas cloud 3/30 s later.

TABLE 1

Simulation design parameters

Parameter	Scale[a]								
	Full	1:50		1:100		1:300		1:500	
Release height (m)	13	0.26		0.13		0.043		0.026	
Release width (m)	14	0.28		0.14		0.047		0.028	
Release volume (m^3)	2000	0.016		0.002		7.4×10^{-5}		1.6×10^{-5}	
Release volume (L)	2×10^6	16		2		0.074		0.016	
Richardson number	2.1	2.1		2.1		2.1		2.1	
Reference height (m)	10	0.2		0.1		0.033		0.02	
Gradient height (m)	600[b]	12		6		2		1.2	
Density ratio (ρ_g/ρ_a)	1.96	1.96	4.19	1.96	4.19	1.96	4.19	1.96	4.19
Wind velocity at reference height (m/s)	7.5	1.08	1.97	0.75	1.37	0.44	0.80	0.34	0.62
Wind velocity at pilot height (m/s)[c]		1.45	2.65	1.01	1.85	0.59	1.08	0.46	0.84

[a]Thorney Island, Phase I, Trial #13.
[b]Assumed U.S. EPA boundary layer height.
[c]Pitot height in wind tunnel is 1.5 m; assumes 0.11 wind profile.

TABLE 2

Dimensions of instantaneous releases

Parameter	Scale[a]		
	Full	1:50 scale	1:100 scale
Height, H (m)	13	0.276	0.126
Diameter, D (m)	14	0.251	0.142
Volume (L)	2,000,000	13.63	2.0
Aspect ratio, H/D	0.93	1.10	0.89

[a]Instantaneous releases at Thorney Island after [8].

ments run with the 1:100 scale canister, the location of the cloud front was often difficult to determine visually due to the smaller volume of gas.

Still-air releases were carried out over a smooth flat surface (roughness length equivalent to 2 to 5 cm for full-scale, similar to short grass) both with and without obstacles. The obstacles used in this analysis were 7 cm cubic blocks. Although this block size was of the same order as the canister size, observations showed that the block size was generally much larger than the cloud height at the distance of interaction. Two different obstacle configuration arrays were studied—termed full-coverage and half-coverage—which are illustrated in Figs. 3 and 4, respectively. Several different obstacle arrangements were tested with

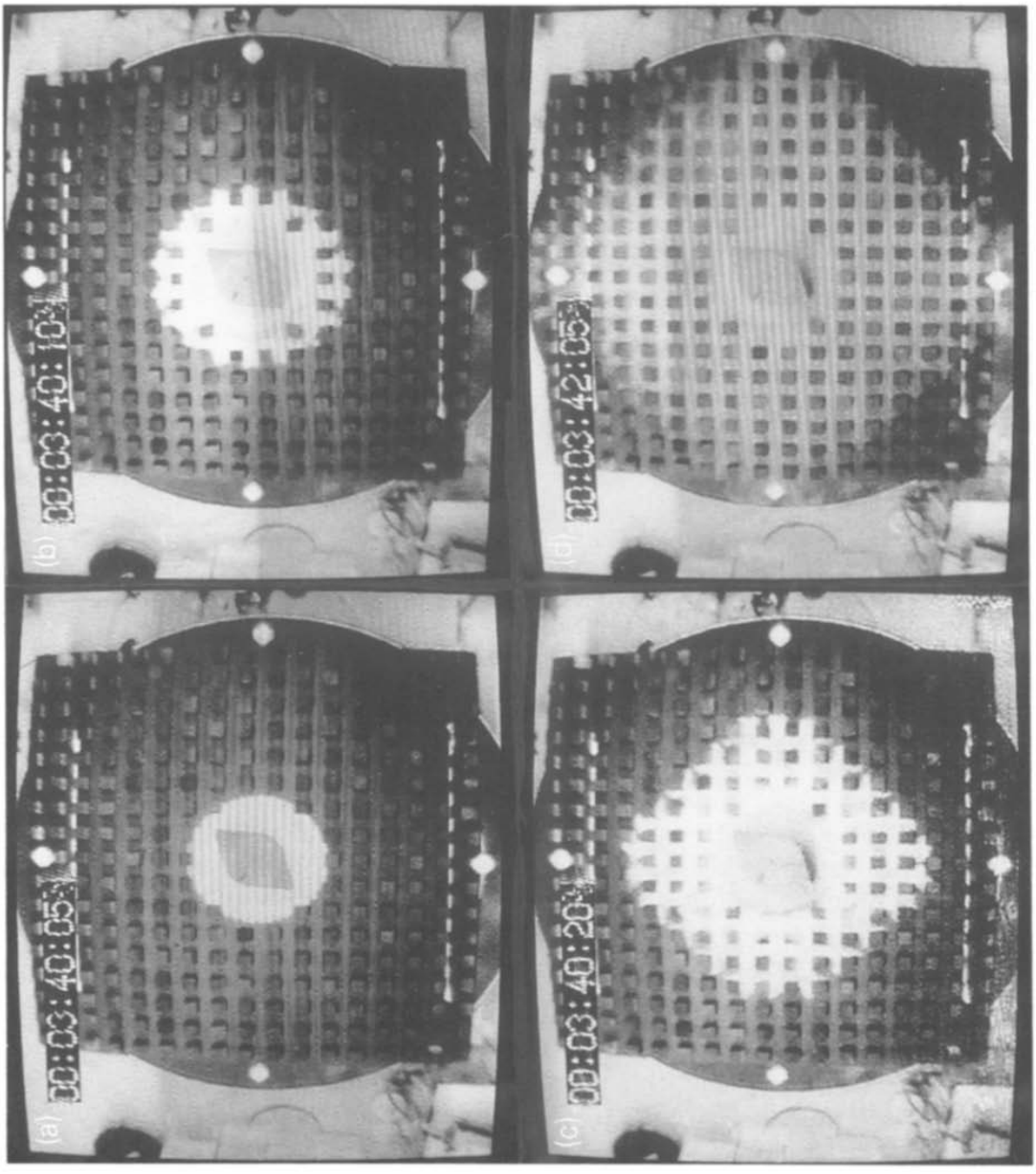

Fig. 3. 1:1 Block spacing with full block coverage.

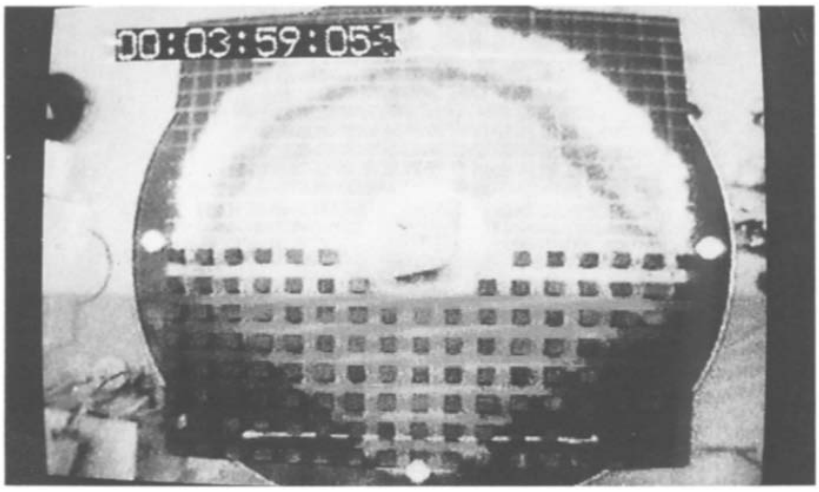

Fig. 4. 1:1 Block spacing with half block coverage.

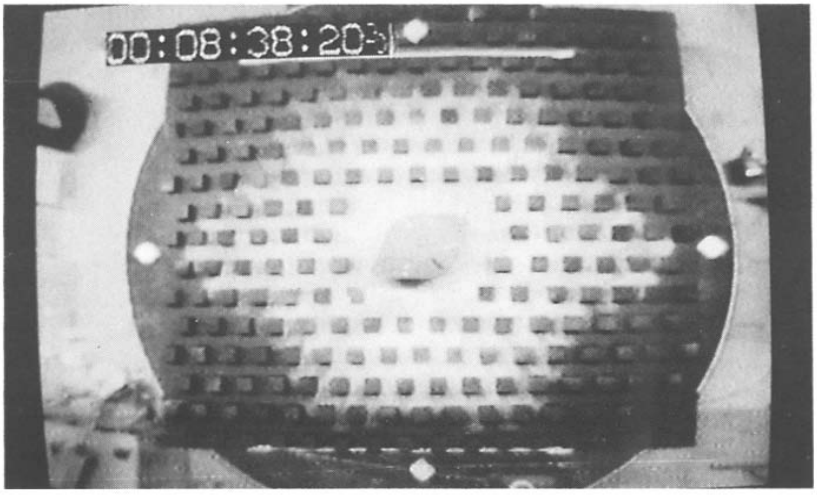

Fig. 5. 1:1 Staggered block spacing with full block coverage.

these configurations. These consisted of variations in obstacle spacing and alignment as follows: three different spacings (0.28:1, 1:1 and 3:1) and three alignments (no blocks, regular and staggered spacings). The spacing ratios given here indicate the width of the space between the block columns and rows in multiples of the block width/length. For example, the 1:1 spacing indicates that the spacing between the rows and columns is one block width or 7 cm. Only one set of staggered alignment tests were conducted using a 1:1 block spacing. In the staggered spacing, alternate rows are moved to the left one space from the row before (Fig. 5).

3.2 Flow visualization methodology

Detailed visual records of the flow path of the cloud for all releases were obtained by video cameras mounted directly overhead and to the side of the

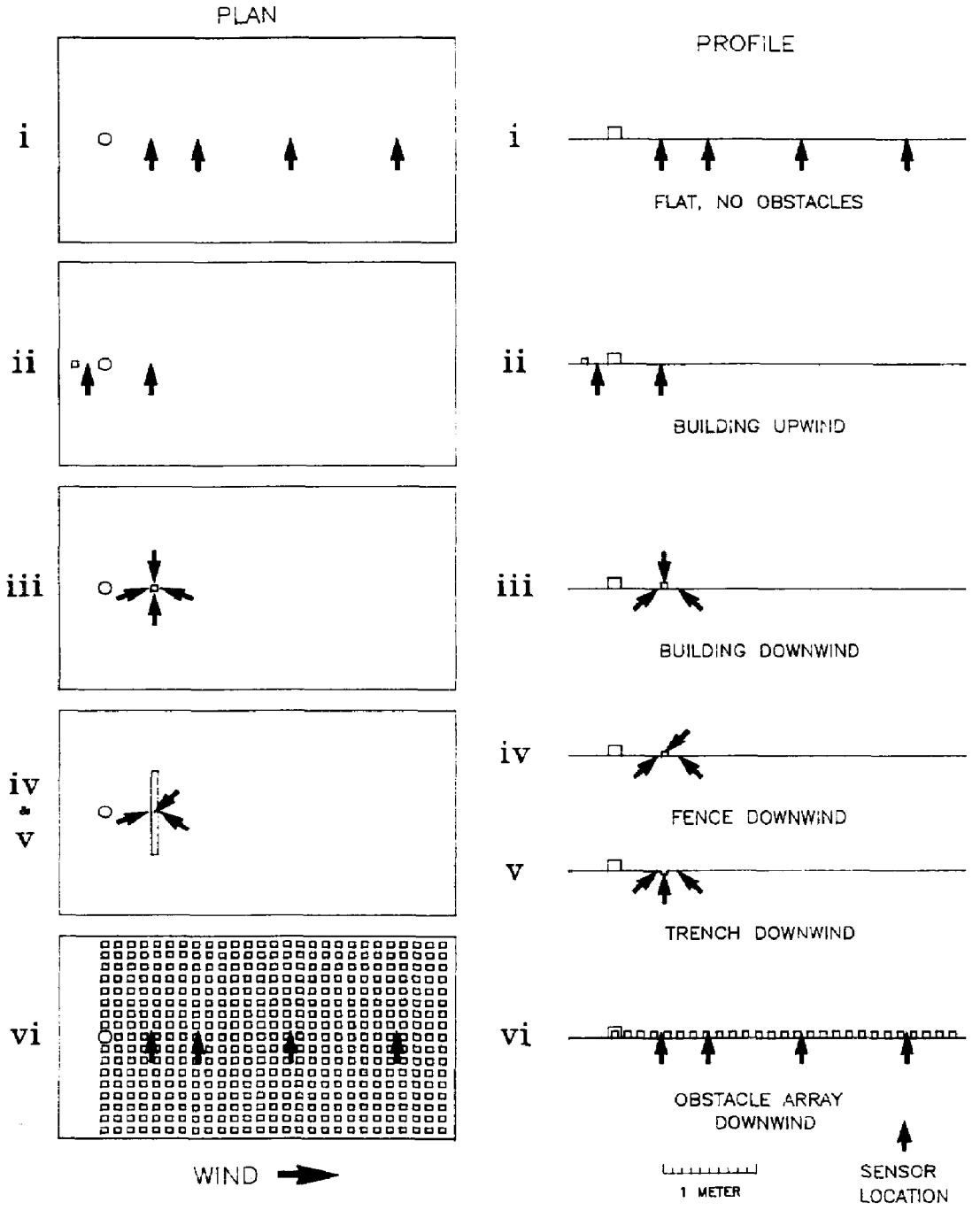

Fig. 6. Test configurations for obstacle array experiments.

release canister. These provided a continuous record of both bird's-eye and profile views of the gas cloud dispersion. A time indicator was added to the video tapes of the releases and selected frames of the tapes photographed for cloud spread analysis. In the still-air experiments, the distances of the heavy gas cloud front from the center of the release cylinder were measured on these photographs and converted to full model scale to determine the time history of the cloud spread.

3.3 Concentration measurement trials

Gas concentration measurements were made with the following special obstacle test configurations at 1:100 model scale as illustrated in Fig. 6 (note, dimensions are given in full-scale equivalents):

(i) flat terrain with no obstacles, similar to Thorney Island Release #13;
(ii) single 14-m cubic obstacle located 29 m upwind of release center;
(iii) single 9-m cubic obstacle located 50 m downwind of release center;
(iv) a 5-m high fence located 50 m downwind of release center;
(v) a trench located 59 m downwind of the release with dimensions 7 m across 3.5 m deep by 100 m wide; and
(vi) a uniform array of obstacles (7-m cubes spaced 7 m apart) located downwind of the release center.

Concentrations were measured with each configuration at tunnel wind speeds of 0, 0.8 and 1.2 m/s at a height of 10 cm which correspond to calm, 7.4 m/s and 11.1 m/s wind speeds at full scale height of 10 m. (Hereafter, wind speeds will be referred to in the full-scale equivalent unless otherwise noted.) The gas cloud was a mixture of air and sulfur hexafluoride (SF_6) and marked with a water–glycol based smoke. Based on Richardson scaling, the mixed gas densities used in the simulated releases were 2.4 and 3.9 kg/m^3. The atmosphere in which these simulations were performed was considered to be indicative of neutrally stable atmosphere. No attempt was made to simulate flows in either stable or convective atmospheres.

4. Flow visualization of still air releases with regular obstacle arrays

An overhead view of the heavy gas cloud spreading in zero wind conditions and no obstacles (Fig. 7) showed a very uniform circular spreading pattern with radius increasing with time. This cloud was similar to that observed at full scale under near calm wind conditions in the Thorney Island Trials and under low wind conditions and in the wind tunnel experiment of Hall and Waters [9,10]. The cloud shows a rather billowy outer ring, a mostly clear area behind the ring and a denser cloud behind the clear area shortly after release. When viewed from other angles, it is obvious that the cloud front is shaped as a toroidal ring rather than a uniform cylinder—a shape assumed in most mathematical box models of heavy gas dispersion.

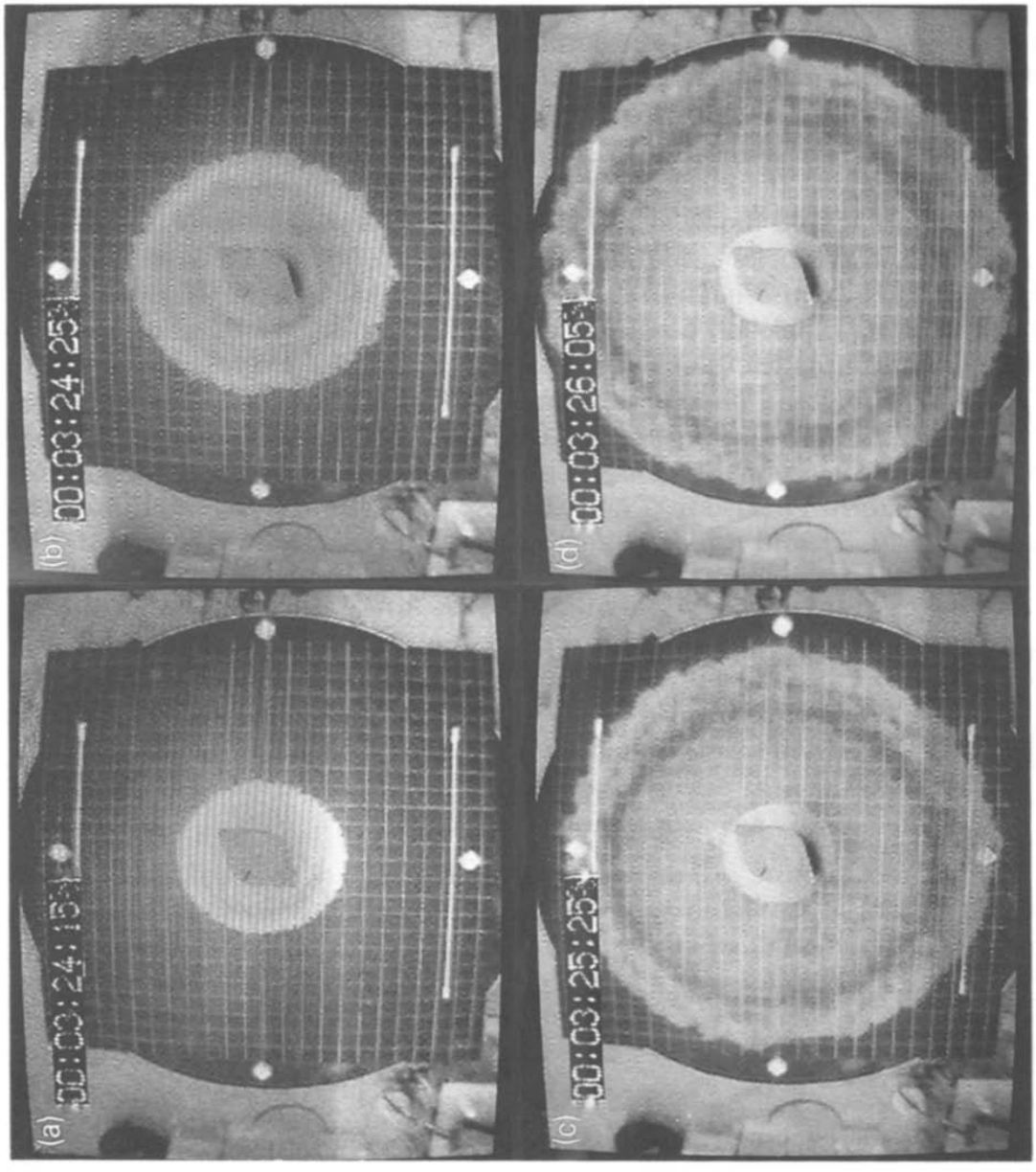

Fig. 7. Sequence of heavy gas spread under "no blocks" condition.

4.1 Cloud spread for 1:1 block spacing, full coverage scenario

With 1:1 block spacing and full coverage (Fig. 3), the released gas initially spreads as a circular cloud. After some time, however, the gas in the cloud moving through the blocks begins to lag behind the gas moving along the horizontal and vertical corridors. On the 45° diagonal this lag is the greatest. The resulting flow pattern is an expanding diamond with corners along the corridors.

4.2 Cloud spread for 1:1 block spacing, half coverage scenario

The cloud spread under this scenario (Fig. 4) is similar on the lower half to the flow in the full coverage case, while the upper half is similar to the no blocks scenario. The resulting figure is a half diamond below and semicircle above. Of interest here is that the radii of the semicircle and the distance down the 90° corridor through the blocks are the same.

4.3 Cloud spread for 1:1 staggered block spacing, full and half coverage scenarios

In these 1:1 staggered block, full- and half-coverage scenarios (Figs. 5 and 8, respectively), the blocks remain spaced as in the above 1:1 scenarios but with alternating rows of blocks is shifted one space to the left. This leaves an repeating block–no block–no block pattern as the ranks are descended. This pattern also eliminates the block-free central corridor. As a result, the cloud moves furthest along the obstruction-free horizontal corridors. The vertical spread travels a similar distance down a number of alternate routes, but because of the obstruction of the blocks, cannot move as far radially as the flow through the horizontal corridor. The resulting patterns are hexagonal for the full coverage (Fig. 5) and a half hexagon below and semicircle above for the half coverage (Fig. 8).

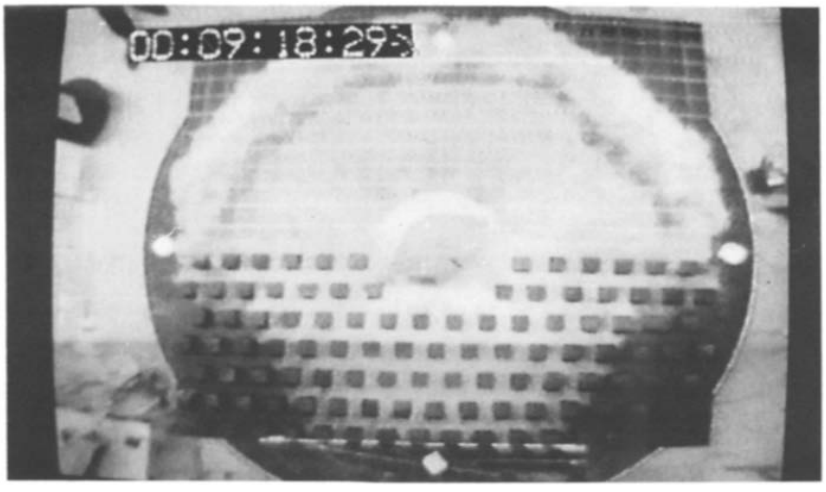

Fig. 8. Sequence of heavy gas spread under 1:1 staggered block spacing with half block coverage.

The difference in the shapes for the 1:1 release under regular and staggered arrays may be accounted for in the additional distance over which a parcel of gas moves through the blocks after release. In the two arrays considered, let us assume the rate of movement of the cloud front through the blocks is constant for a given block density. If the rate of movement (speed) is constant, then the distance the cloud front will travel for any given time after release will be the same for all parcels. Those parcels travelling down the unobstructed corridors will, of course, travel the furthest. Those required to find a path through the blocks will have a more circuitous route and therefore will travel a shorter radial distance from the canister.

This effect is readily observed in the comparison of the cloud spreads between the 1:1 block coverage with the regular array pattern and the 1:1 coverage with the staggered coverage. The only difference between these arrays is that for the staggered array every other row is offset by one block width. The effect of this stagger is that the open corridor which runs vertically for the regular 1:1 array is obstructed by blocks.

Figure 9 is a simplified diagram comparing these two arrays. Only the bottom half of the array is shown; the top half is either the mirror image or empty depending on whether the block coverage is full or half. Let us assume that the cloud parcel leaving from Point O moves at a speed of one block width per time unit. After 13 time units, that parcel would have moved to one of the indicated end points. In the regular array (Fig. 9a), the flow down the horizontal and the vertical corridors, unobstructed for 13 spaces, ends at Points A. For flow down the diagonals (e.g. to Points B), the parcel may traverse any of several paths which total 13 spaces in length. The resulting pattern (denoted by the heavier dots) is a half diamond.

For the staggered array (Fig. 9b), the unobstructed path to Points A is only possible along the horizontal corridor. Since the cloud moving "downward" on the diagram no longer has a clear run, the cloud must pass around several blocks. As a result, after 13 time steps any one of the Points B may be reached. End points between A and B denote different pathways. In this case, the resulting pattern is half of a hexagon similar to that shown in Figs. 5 and 8 for the staggered block array.

4.4 Cloud spread for 3:1 block spacing, full coverage scenario

In the 3:1 block spacing (Fig. 10), the blocks have a minimal effect on the flow pattern until long times after release. The pattern begins as a circle and remains that way for at least the first second after release. Some scalloping of the cloud is evident around the blocks as the gas is diverted around them. After one second, the shape begins to take a diamond pattern although it never reaches the distinct diamond pattern of the 1:1 spacing before reaching the edge of the study platform.

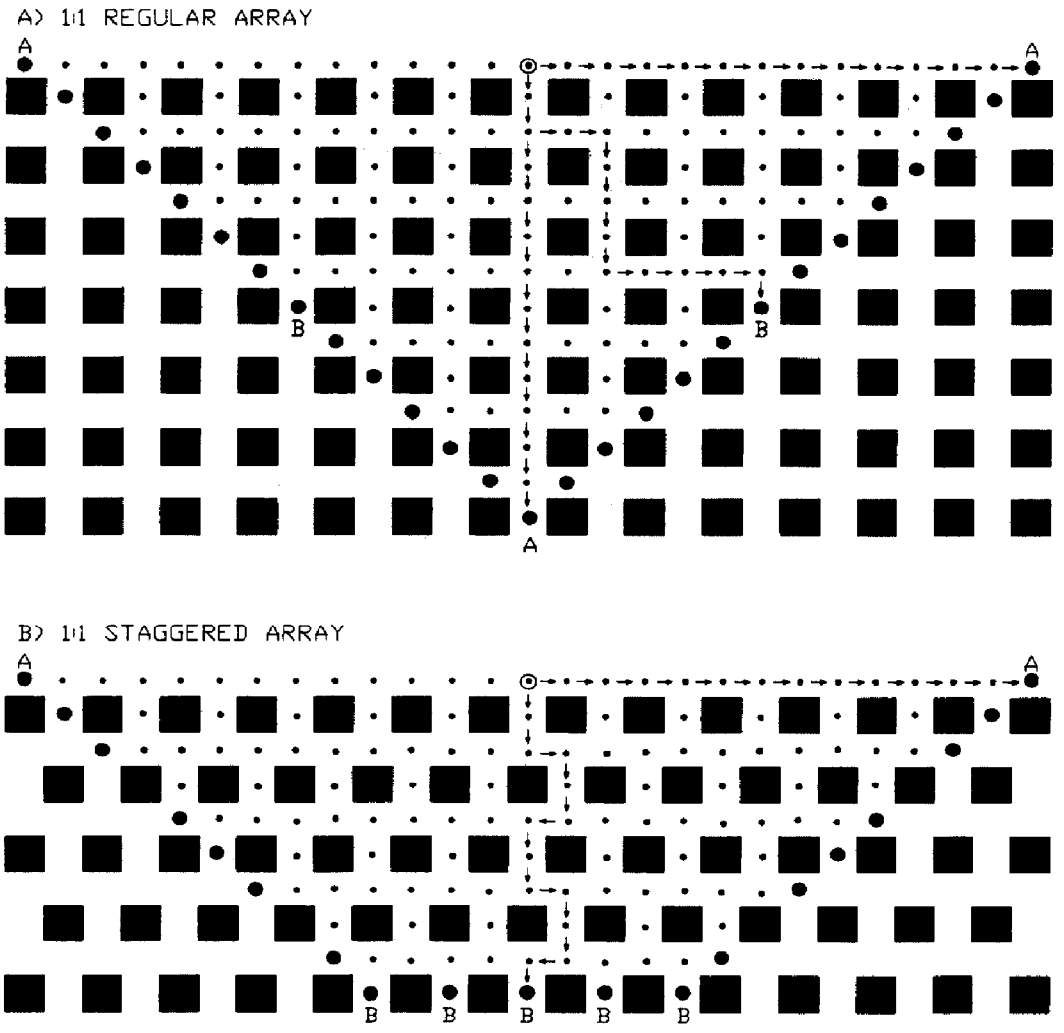

Fig. 9. Sequence of heavy gas spread under 3:1 block spacing with full block coverage.

4.5 Cloud spread for 0.28:1 block spacing, full coverage scenario

With the 0.28:1 block spacing (Fig. 11), the flow pattern is complicated by the nearness and density of the blocks at the release point. Upon release of the gas, the cloud rapidly slumps to fill the blockless region surrounding the canister. When viewed from a lower angle and closer to the release area (Fig. 12), the gas cloud is seen to flow over and against the blocks like a wave breaking against a sea wall. Portions of the cloud then reflect back toward the opposite side of the clear area while some cloud material enters into the spaces between the blocks. The cloud material is also observed to slosh within the clear area for several oscillations. As a result, two clouds are observed: one which moves between the blocks producing first a circular and then a diamond pattern, and one which travels above the blocks as a quasicircular cloud. The upper cloud

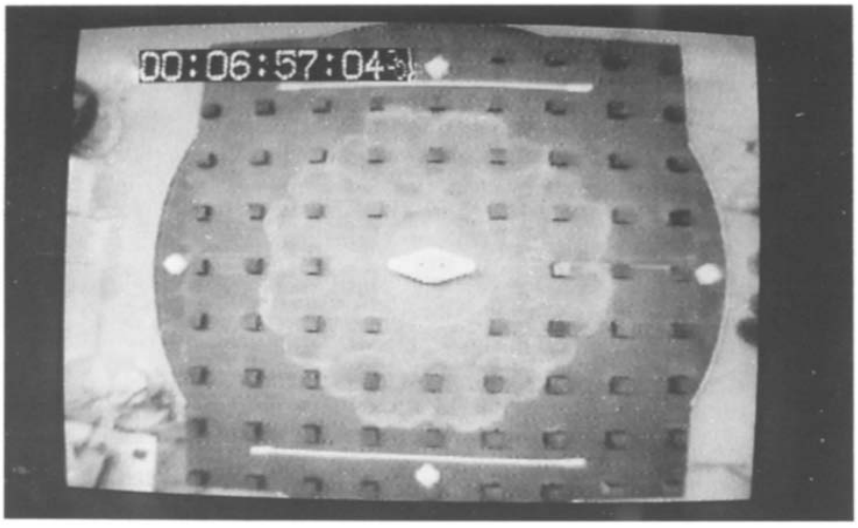

Fig. 10. Sequence of heavy gas spread under idealized flow through two 1:1 block configurations: (a) regular array, and (b) staggered array.

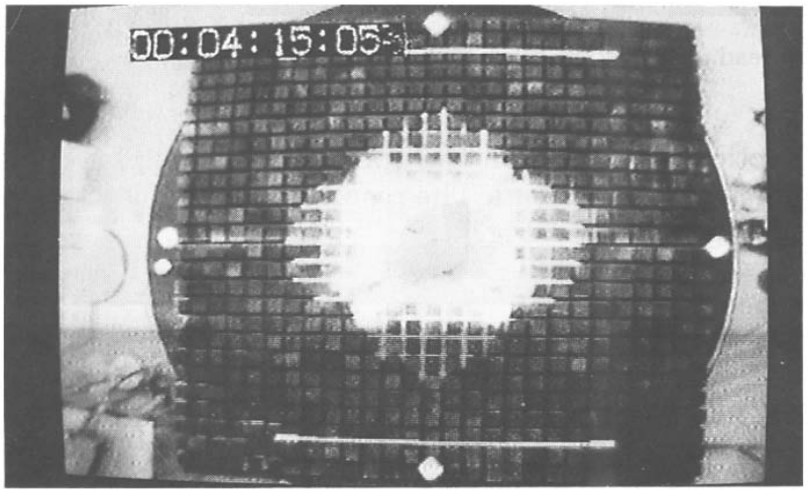

Fig. 11. Sequence of heavy gas spread under 0.28:1 block spacing with full block coverage.

is much brighter optically on the flow visualization photographs, but the lower cloud is evident by its outlining of the blocks which the gas surrounds. The lower cloud moves faster in the still air. Much of the upper cloud remains close to the source and eventually much of it sinks into the spaces between blocks to join the lower cloud. Some of the cloud, however, may mix with the ambient air and its density lowered so that it may disperse as a passive cloud.

The pattern with half-coverage (not shown) is similar to the 1:1 half coverage with the addition of some flow over the blocks on the covered half with the initial release wave. Reflection of material from the blocks drives gas up-

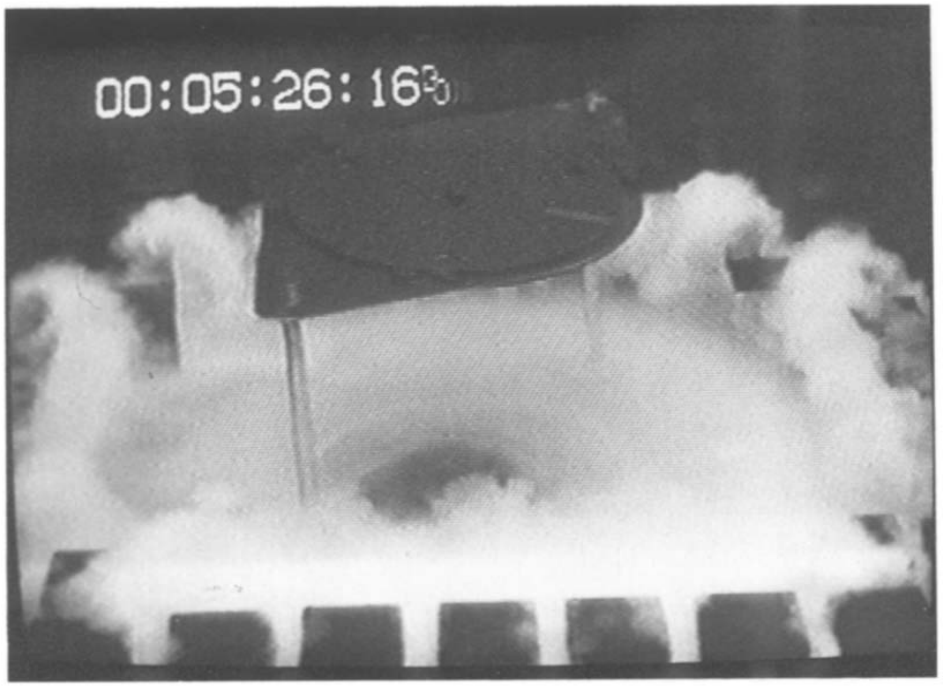

Fig. 12. Sequence of heavy gas spread under 0.28:1 block spacing with full coverage—close up of release area.

ward, but without the reflection off blocks on the upper half of the platform, there is no return or sloshing of the gas cloud. The resulting pattern is similar to that for the 1:1 half-coverage shown in Fig. 4.

5. Flow visualization for special obstacles

5.1 No obstacles

An overhead photo of the first test configuration is shown in Fig. 13 after a release under low wind conditions (7.4 m/s full-scale wind speed at 10 m height). The spreading is strongly influenced by the wind as it shears the top and sides of the cylindrical cloud immediately after the release. As the cloud slumps, some gas moves into the wind and then is pushed back downwind. Although not shown, at a higher wind speed (11 m/s), the extent of upwind movement is very small.

5.2 Single block upwind

In the second test configuration, a single 14-m block (e.g. a building at full scale) located 29 m upwind of the center of the release, is shown in Fig. 14. With the wind blowing from right to left in the figure, the low pressure zone on the downwind side of the building has caused the cloud front to rapidly travel upwind into the low pressure zone. Subsequent erosion of this cloud took

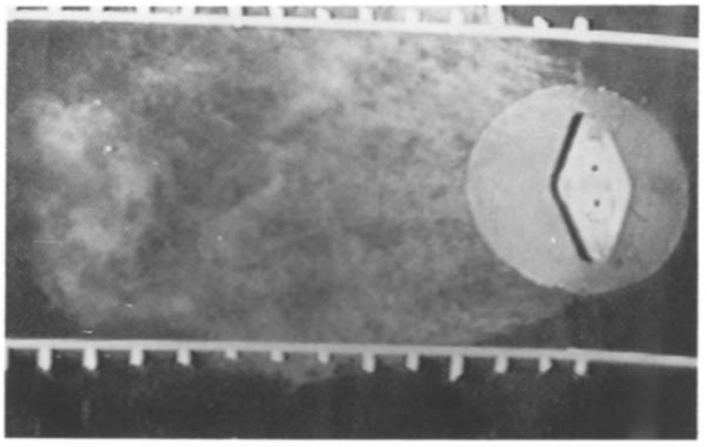

Fig. 13. Test configuration (i): Cloud spread without obstacles at 1:100 scale under low winds.

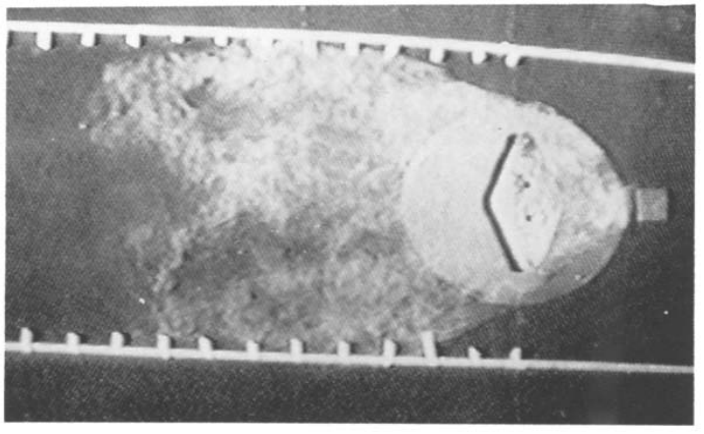

Fig. 14. Test configuration (i): Cloud spread—Single obstacle upwind of release.

a significantly longer period of time than for the upwind portion of the heavy gas cloud without the obstacle (e.g., Fig. 13).

5.3 Single block downwind

The cloud pattern just after release with a single 9 m block located 50 m downwind from the centerline is shown in Fig. 15. The presence of the obstacle divides the cloud down the center, and under wind speeds of 7.4 m/s, the cloud flow is often not symmetrical. As observed in Fig. 15, the bulk of the cloud mass appears to move past the building on the upper part of the photo. Based on observations from other replicate releases, it is likely this asymmetry is a result of slight meander in the wind stream.

5.4 Fence downwind

Overhead photos taken with a 5 m by 5 m by 100 m wide fence located 50 m downwind from the release center are presented in Figs. 16 and 17 for calm

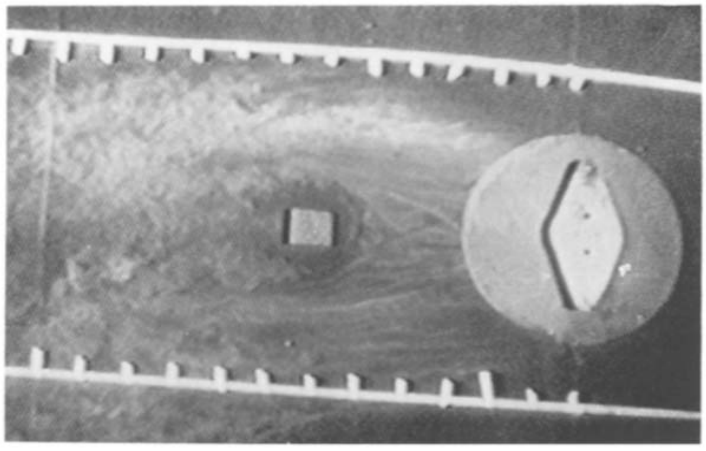

Fig. 15. Test configuration (ii): Cloud spread—Single obstacle downwind of release.

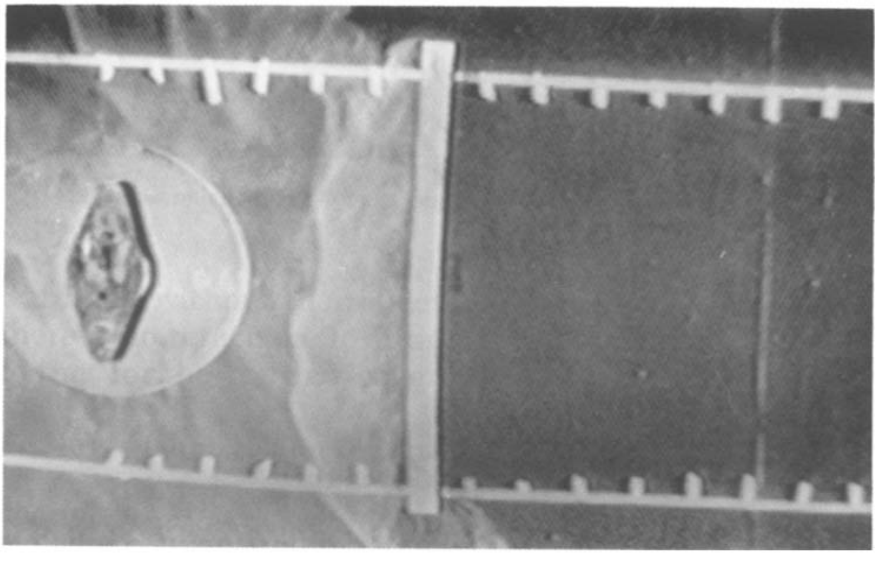

Fig. 16. Test configuration (iii): Cloud spread—fence downwind of release—calm conditions.

winds and low winds (7.4 m/s), respectively. Under calm conditions, the fence is effective in blocking the cloud path. The cloud bounces back from the fence in a strong reflection wave. This reflection is clearly illustrated in Fig. 16. Note, very little gas moves over the fence under the calm condition. In the low wind case shown in Fig. 17, a reflection is also observed, however, the cloud eventually passes over and around the fence. With winds of 11 m/s (not shown), the cloud passed over the fence with very little cloud mass moving around the fence ends.

5.5 Trench downwind

An overhead photo of a release with a trench of dimensions 7 m across by 3.5 m deep by 100 m wide is shown in Fig. 18 under a wind speed of 7.4 m/s.

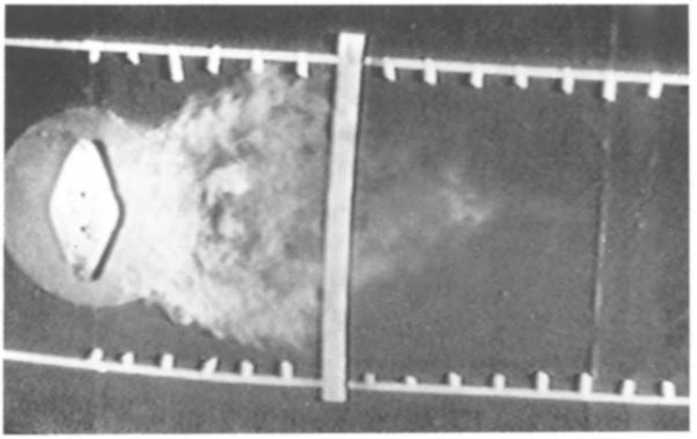

Fig. 17. Test configuration (iv): Cloud spread—fence downwind of release—under low winds.

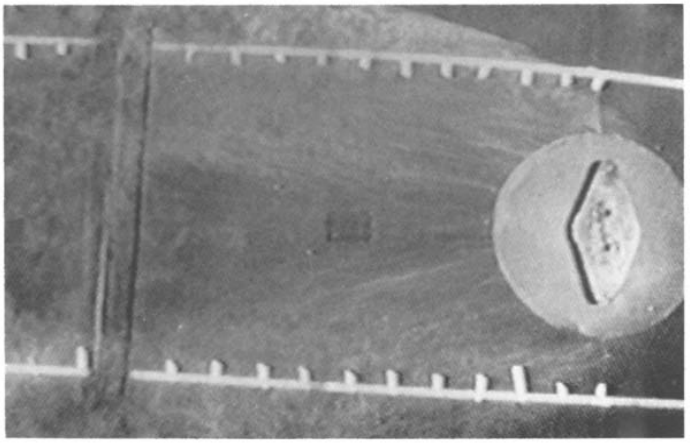

Fig. 18. Test configuration (v): Cloud spread—trench downwind of release—under low winds.

The cloud flowed into the trench and was observed to roll over in the trench entraining clean air and then completely clear shortly thereafter. This phenomenon was observed at both tested wind speeds (7.4 m/s and 11 m/s). With no wind, the trench was observed to fill with gas which small turbulent eddies eventually evacuated.

5.6 Uniform block array downwind

Overhead and side-view photos just after a release with a uniform array of obstacles downwind of the release are shown in Figs. 19 and 20, respectively. Similar to observations under calm winds, the cloud front moved faster down the block-free corridors than in a direction away from the downwind vector. As shown in Fig. 19, the wind drives the cloud flow and the interaction of the cloud with the obstacles at the edge of the cloud causes the cloud to be redirected away from the general wind direction. Flow down the corridor parallel

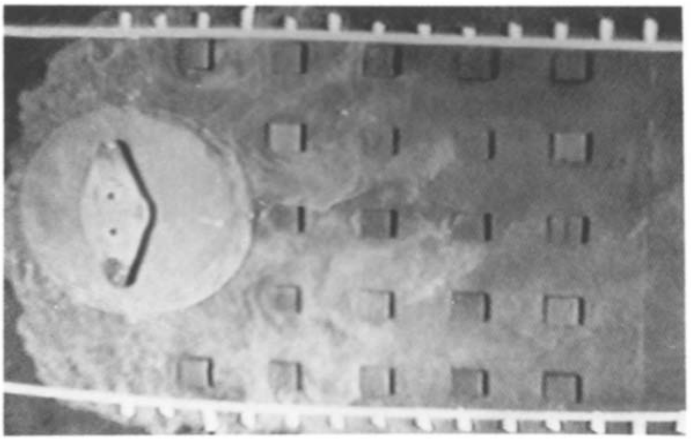

Fig. 19. Test configuration (vi): Cloud spread—uniform array of obstacles downwind of release—under low winds—overhead view.

Fig. 20. Test configuration (vi): Cloud spread—uniform array of obstacles downwind of release—under low winds—side view.

with the tunnel centerline proceeds much more rapidly. Under high wind conditions, the effect of the obstacles was less obvious. The cloud shape was very similar to releases in terrain with no obstacles.

5.7 Summary

The observations made from the video records of the heavy gas cloud dispersion in the absence and presence of obstacles indicate:

(i) the presence of obstacles significantly altered heavy gas cloud behaviour under calm and low wind conditions within 50 m of the release;

(ii) as wind speed increased, the presence of obstacles had decreasing observable influence on the cloud shape;

(iii) movement of the cloud front in an upwind direction into the lee of a single block building was more rapid than the upwind spread when the building was not present;

(iv) the fence located downwind of the release acted as an effective barrier under calm wind conditions; the effectiveness decreased with increase in windspeed; and

(v) the presence of a uniform array of obstacles influenced the cloud behaviour near obstacles, but in an overall sense, the changes were not too large; the influence of obstacles was stronger at the lower windspeeds.

6. Concentration profiles for flow through special obstacle arrays

Six experiments were performed using the 1 : 100 scale canister with differing obstacles to determine their effect on concentration profiles and cloud movement. The density of the gas used in the experiments reported herein was 2.4 kg/m^3 and the wind speed was 7.4 m/s full scale. Data from these experiments is presented in Table 3. All times and distances are converted to full scale. In Table 3, the location of the FID probe is indicated along with the initial time

TABLE 3

Summary of FID experiments (All experiments with 2.4 kg/m^3 density and wind speed of 7.4 m/s full scale)

Experiment configuration	Full scale probe location (x,y,z) (m)	Full scale time (s)		Peak concentration ratio (C/C_0)
		Cloud arrival	Peak arrival	
No obstacles	50, 0, 0.4	14	15	0.19
Building 29 m upwind of release	50, 0, 0.4	6.5	7.5	0.55
	−27, 0, 0.4	10	15	0.13
Building 50 m downwind of release	48, 0, 0.4	12	15	0.10
	61, 0, 0.4	15	18	0.022
Fence 50 m downwind of release	57, 0, 0.4	26	53	0.013
	48, 0, 0.4	13	15	0.133
Trench 50 m downwind of release	51, 0, 0.4	13	17	0.185
	59.5, 0, −2.4	18	45	0.085
Uniform block Array—3.5 m Blocks	50, 0, 0.4	9.6	10.4	0.39
	100, 0, 0.4	23	24.8	0.69
	35, 35, 0.4	14.4	20.8	0.15

of cloud arrival, the time of the concentration maximum and the measured maximum concentration ratio (C/C_0) where C_0 is the initial concentration in the canister. The probe locations x, y, z refer to the centerline distance downwind from the center of the release, the distance from the centerline in the across-wind direction, and the height above grade respectively, units are in meters full scale.

6.1 No obstacles

For comparison purposes, full scale Thorney Island Trials #13 and #18 were compared with test configuration (i) results. The data obtained in the wind tunnel are compared with the full scale data for Trial #13 in Fig. 21. The model-scale velocity of 0.8 m/s at 10 cm height (equivalent to 7.4 m/s at 10 m height, full scale) used in the simulation was based on Richardson number scaling, and the time scaling factor was based on the windspeed and the length scale. The concentration was measured at a downwind centerline distance of 50 m and a height of 0.4 m above grade. As shown in Fig. 21, the arrival and departure times of the Thorney Island Trial #13 were well simulated. The concentration time history was also similar in all respects to the Trials except for a sharp peak observed initially. After repeating this experiment three times (Fig. 22), it was thought that the fast instrument response and meander of the cloud may sometimes combine to produce a high peak. The measurements were averaged over a full scale time period equivalent to 0.6 seconds, full scale as were done for the Thorney Island data.

Measurements were also made at downwind distances of 100, 200 and 315 m and height of 0.4 m (not shown). The scale-model concentration comparisons with the full scale were generally good, thus, validating the experimental setup and scaling parameters.

6.2 Single block upwind

Concentrations measured under test configuration (ii) building upwind of the release, are shown in Fig. 23. The peak concentration ratio of 0.55 measured in the lee of the building ($x,y,z = -27,0,0.4$) was the highest concentration ratio measured in any of the experiments. It appears that the low pressure zone in the lee of the obstacle caused the cloud to move quickly upwind toward the downwind face of the obstacle with surprisingly little dilution (see Fig. 14). At 50 m downwind from the release, the arrival time was similar to the no-building (or no-obstacle) case, and the peak concentration ratio was also in the same range—10 to 20% of the initial release concentration. These data illustrate the complexity of the interaction between the wind and gas flows around a building located near a release of a gas which is denser than air.

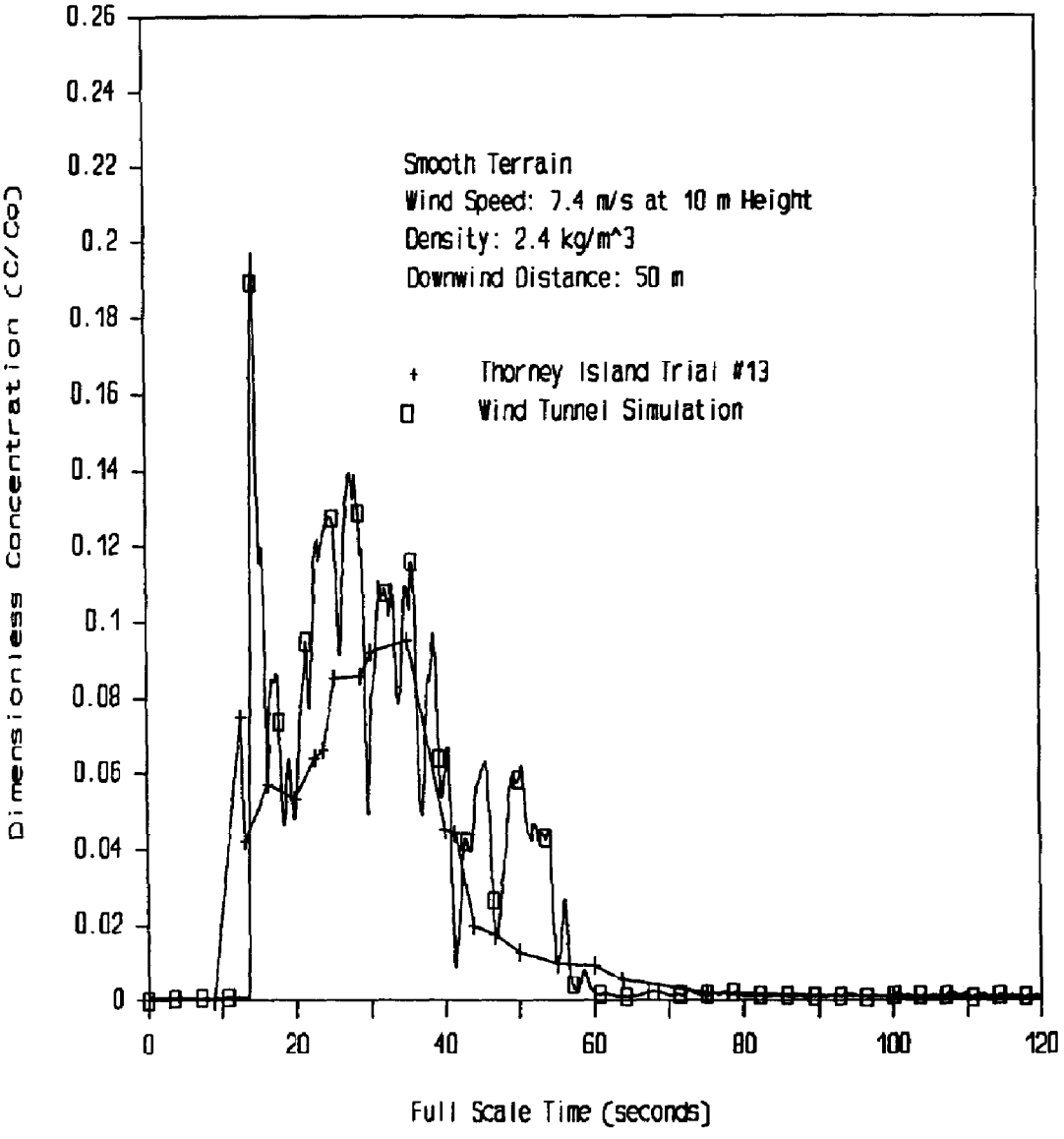

Fig. 21. Comparison concentration history of wind tunnel simulation with Thorney Island Trial #13.

6.3 Single block downwind

Concentration histories are presented in Fig. 24 for test configuration (iii), a 9 m building located 50 m downwind of the release center. The sensors were located just upwind and downwind of the building (48 m and 61 m from the release center, respectively). The upwind concentration peaked at about 10% of the initial concentration and a second peak was observed at about 4%. The downwind sensor peaked at about 2%, decreased to zero, and then returned to about 2% with a slow steady decline to zero thereafter. Although the downwind

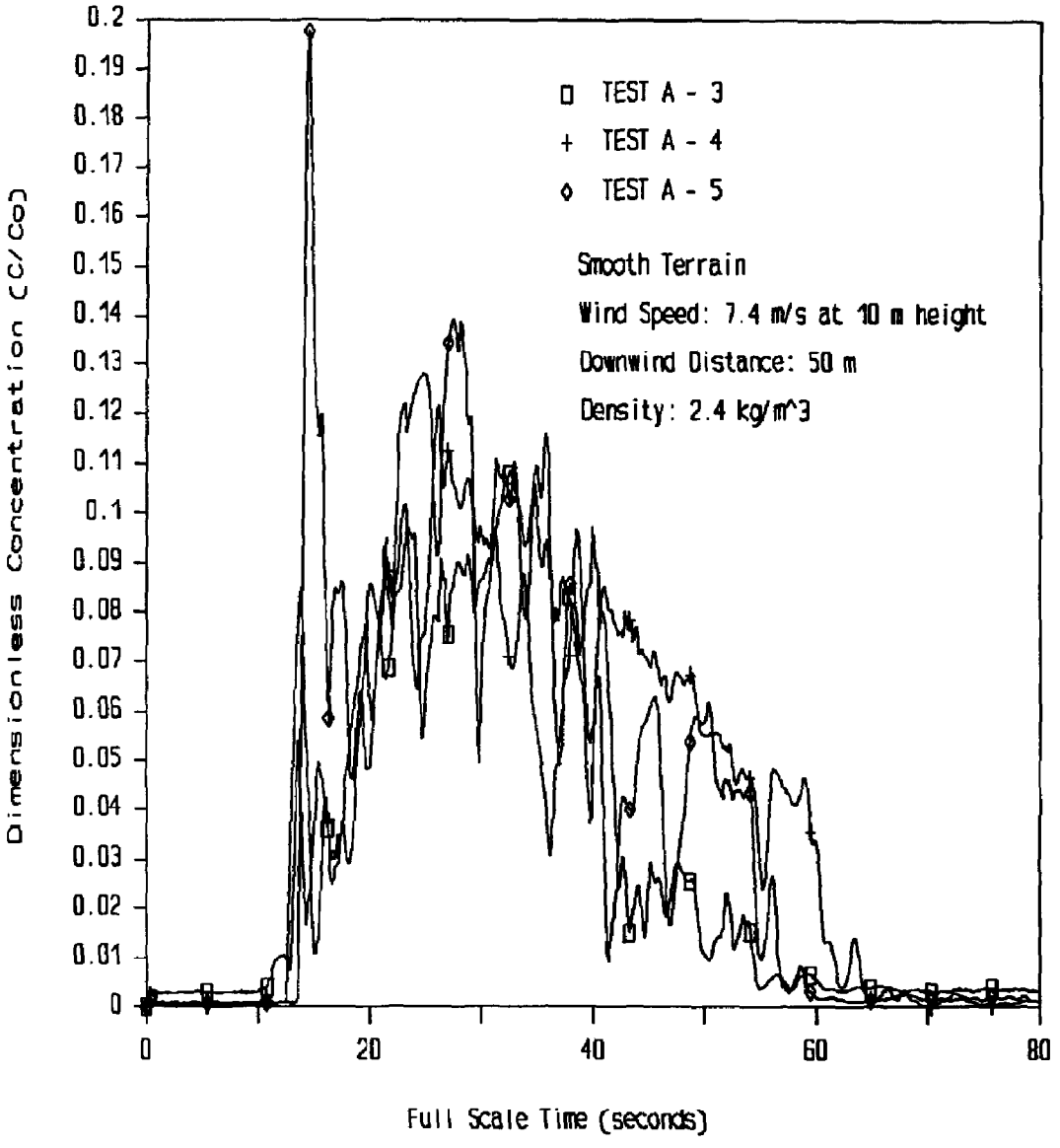

Fig. 22. Wind tunnel replicates of Trial #13—Concentration vs. time.

concentration was about 2%, (a factor of 25 different from the building upwind case), the region on the downwind side of the building appeared to sustain an elevated concentration for an increased period of time. This was similar to the case with the building located upwind of the release.

6.4 Fence downwind

The 5 m high fence located 50 m downwind acted as an effective barrier under calm winds, but as the wind speed increased the cloud moved over the fence more easily. Concentration histories $\rho_g/\rho_a=2$, are shown in Fig. 25 at

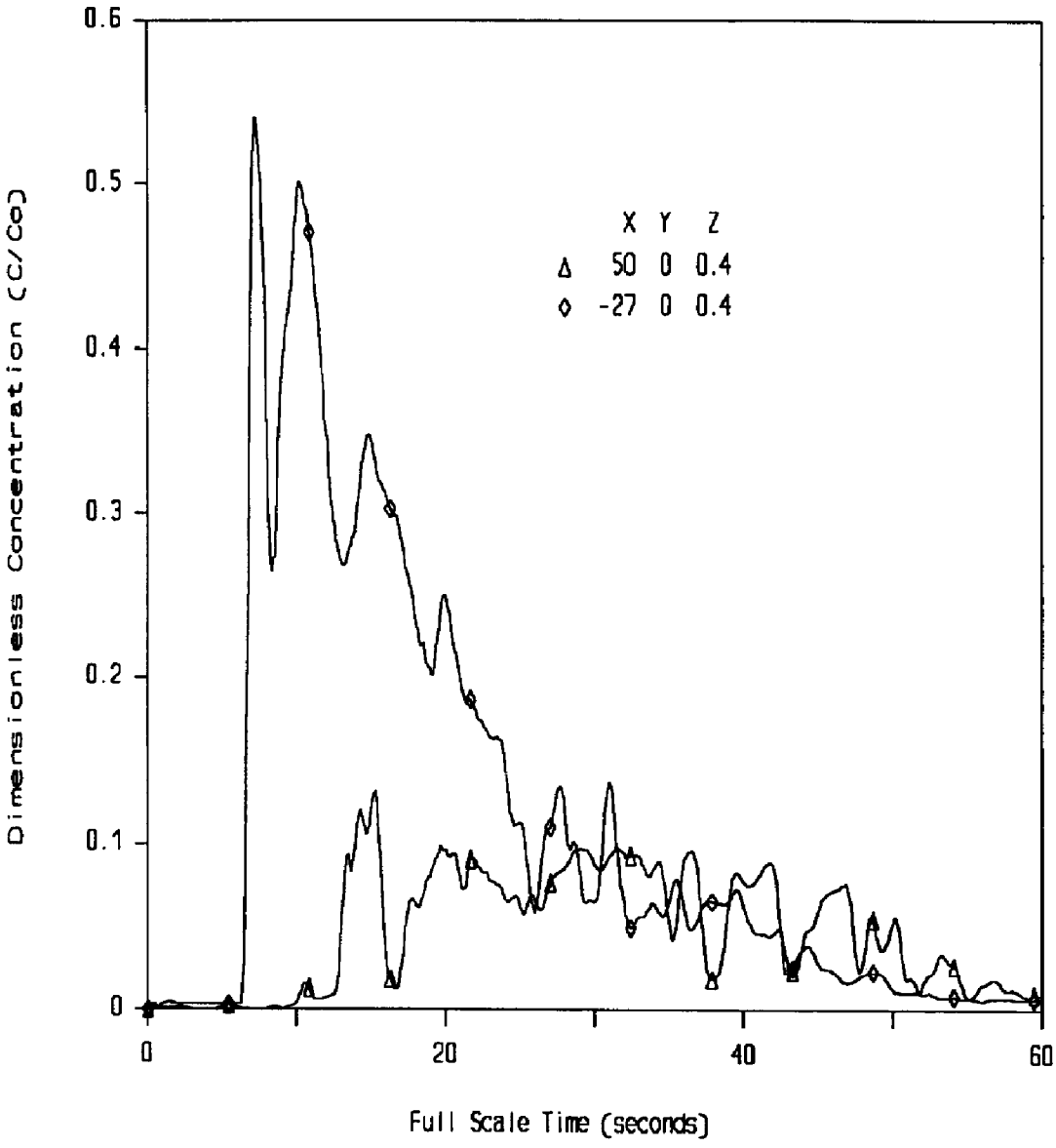

Fig. 23. Concentration vs. time—building 29 m upwind of release center.

points upwind and downwind of the fence. Although not shown here, similar profiles were observed at the 11 m/s wind speed. The arrival time and peak concentration observed upwind were similar to the no obstacle case, but the concentration exhibited a second peak at lower concentration. This may have been the wave reflection from the fence seen clearly in the calm wind photo and not so clearly under low winds. The concentration downwind of the fence was less than 2% of the initial release concentration. This does not necessarily mean the fence acted as an effective barrier. Rather, at the location measured which was close to the ground, the cloud concentration was low.

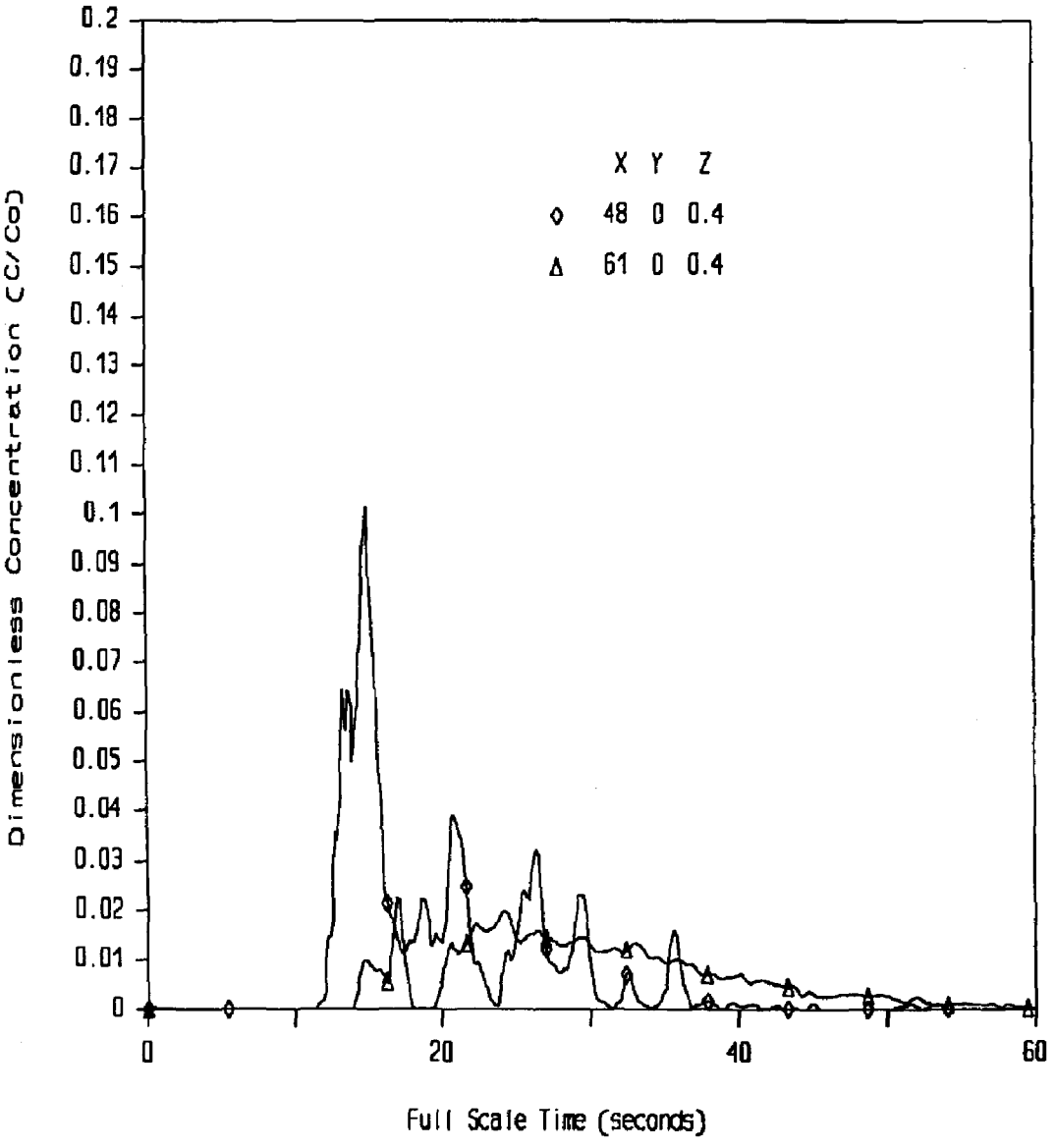

Fig. 24. Concentration vs. time—building 50 m downwind of release center.

6.5 Trench downwind

Histories of cloud concentration measured 5 m upwind of a trench (51,0,0.4) and inside the trench (59.5,0,-2.4) are shown in Fig. 26. The arrival time and peak concentration observed upwind were similar to the case with no obstacles. The cloud arrived in the trench just after the upstream location and a maximum concentration of about 8.5% was observed. The turning or rolling flow in the trench probably entrained air into the cloud thus reducing the peak concentration. The gas clearing from the trench was considerably delayed which supports the observations made with smoke. Similar trends were observed at

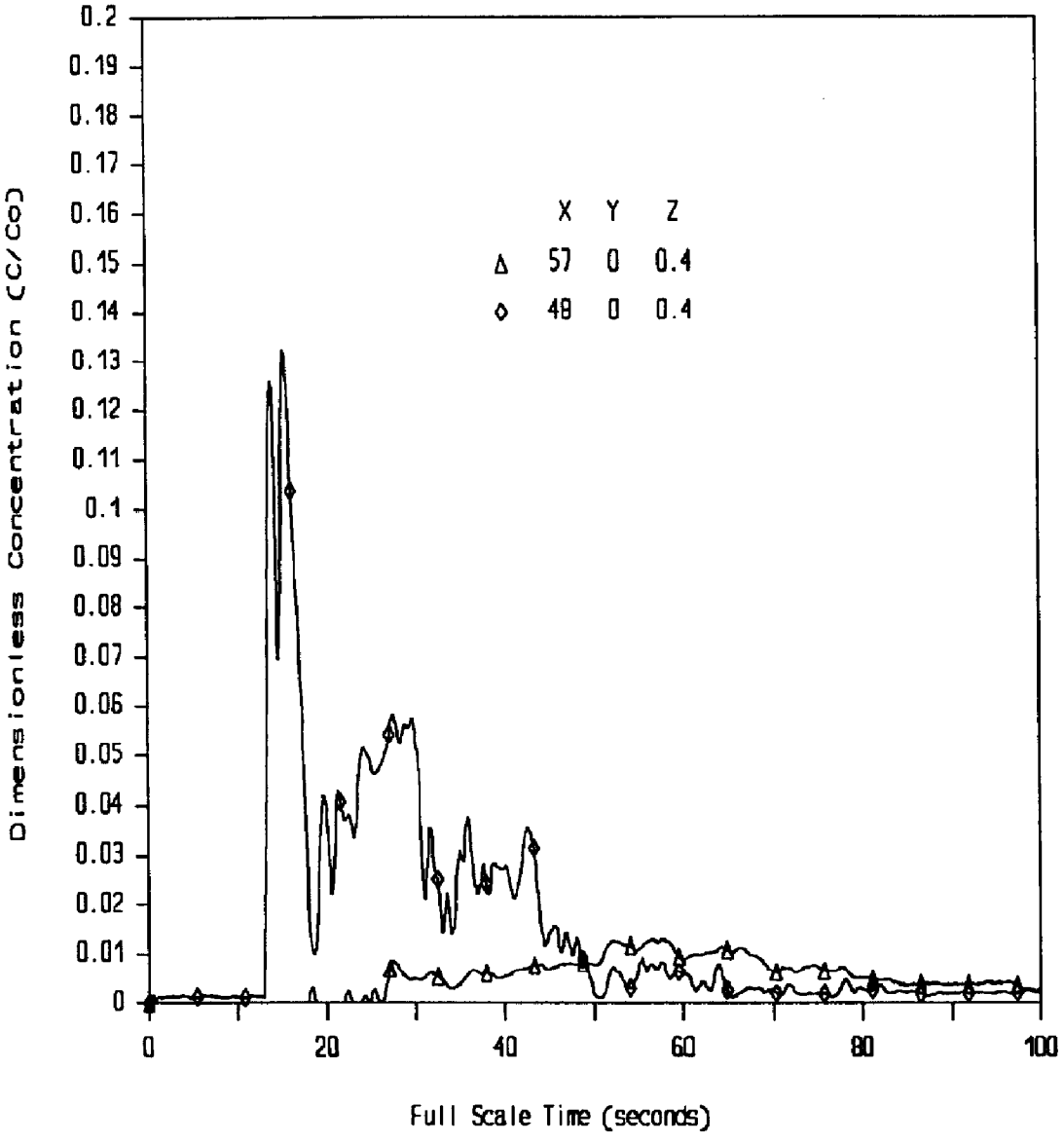

Fig. 25. Concentration vs. time—fence 50 m downwind of release center.

11 m/s. Other tests revealed that an increase in density did not significantly increase the heavy gas residence time in the trench. [1]

6.6 Uniform block array downwind

The concentrations observed with a uniform array of obstacles are shown in Figs. 27 and 28. For distances of 50, 100, 200 and 315 m downwind, the arrival time and departure times are very similar to the case with no obstacles. However, the peak concentration observed at 50 m downwind was significantly higher with the obstacles present. The trace at 100 m was similar to the trace

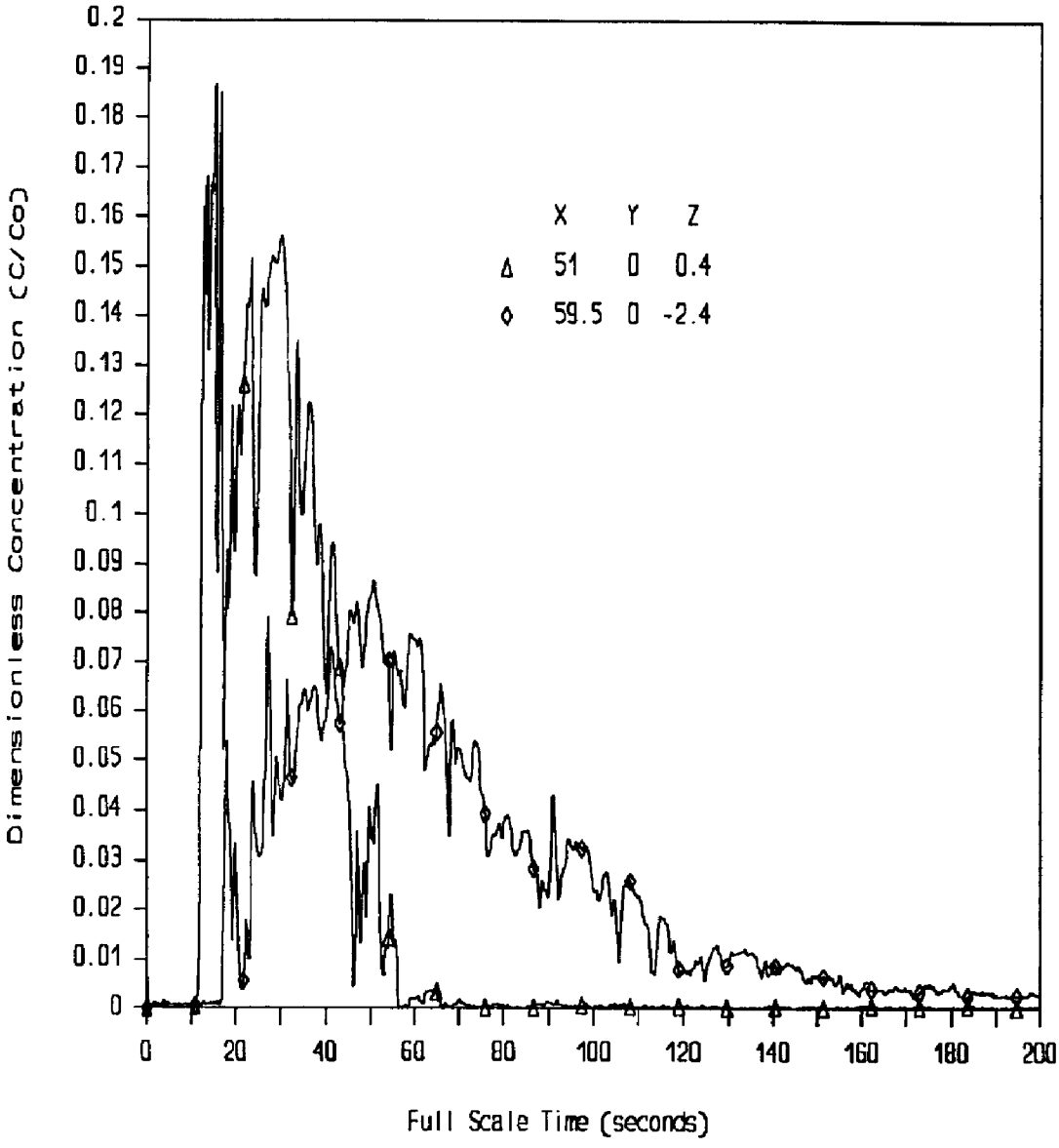

Fig. 26. Concentration vs. time—trench 56 m downwind of release center.

with no obstacles. At 200 and 315 m downwind, the arrival times were similar to the no obstacle case, but peak concentrations were lower. Thus, the presence of the obstacles increased concentration close to the release and decreased concentrations at distances further out. At the higher windspeed, the observed concentrations were much lower than at the lower windspeed, but were similar to the case with no obstacles. It seems the influence of obstacles at the higher windspeed is to decrease the concentration even at distances close to the release (50 and 100 m). At a higher density of 3.9 kg/m^3, the gas concentration decreased more slowly than at the lower density. The arrival time was observed

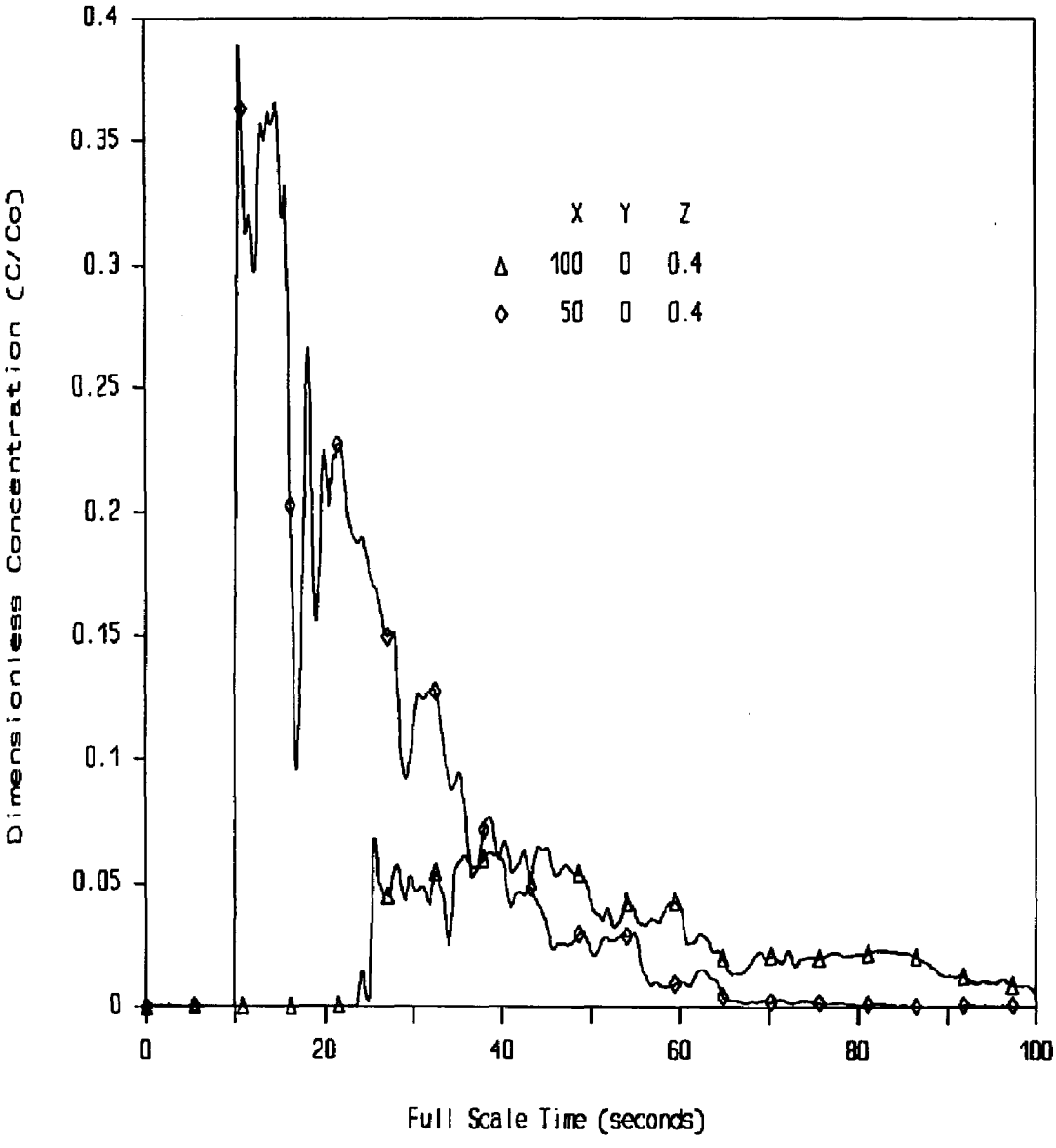

Fig. 27. Concentration vs. time—uniform array of obstacles—flow along corridor.

to increase to 20 s which was thought to be caused by a decrease in acceleration of the heavier cloud immediately after the release.

Concentration profiles taken 50 m directly downwind on the plume centerline and 50 m radius away from the release, but located at a 45° angle from the centerline, are plotted in Fig. 28. In the case of flow away from the corridor, the cloud is forced to move in a more tortuous route around the obstacles. The effect is to delay the arrival time and to reduce the cloud concentration. The reduction in cloud concentration was not too surprising because the sensor was located away from the plume centerline. The delay in arrival time was attrib-

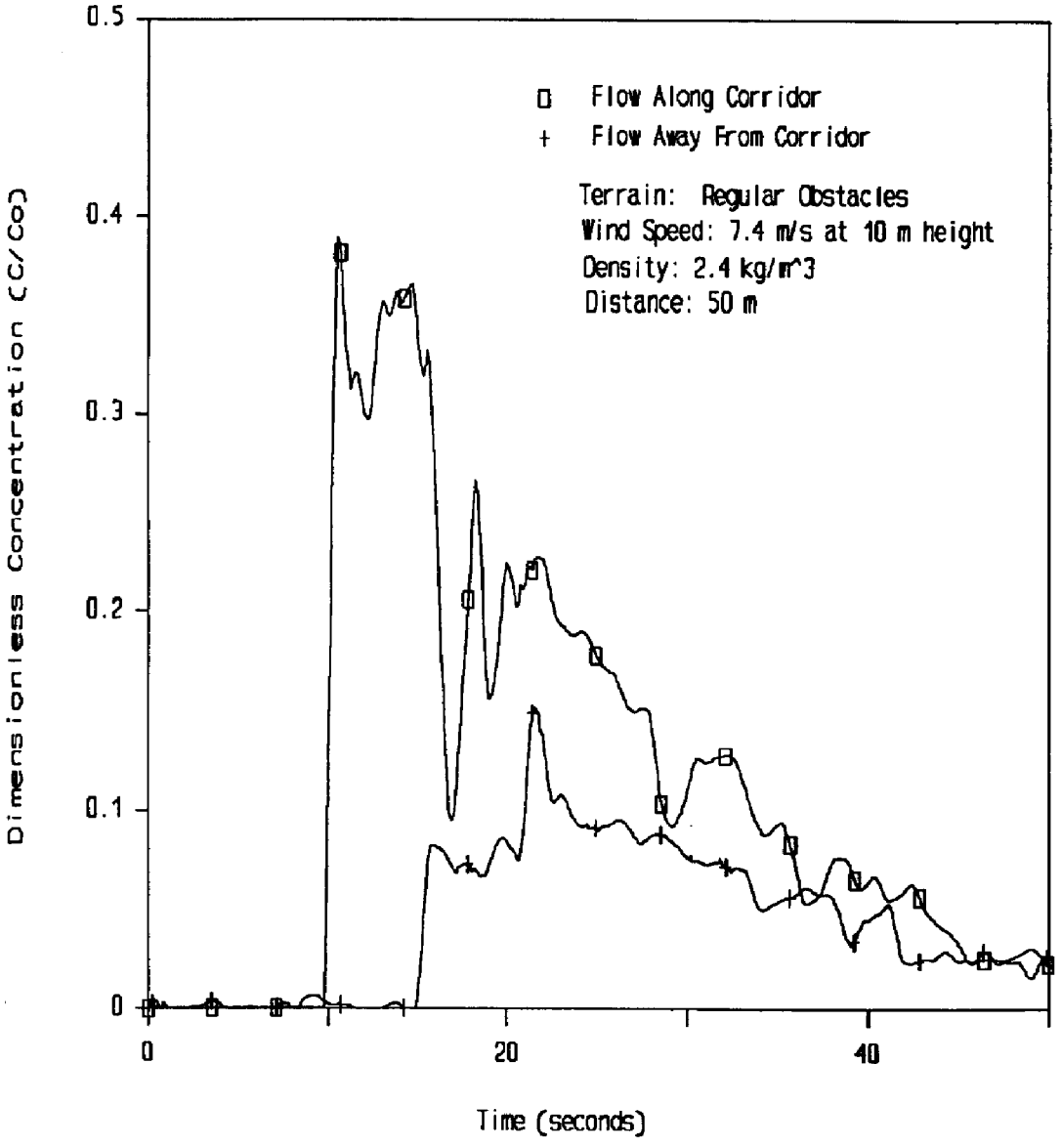

Fig. 28. Concentration vs. time—uniform array of obstacles—effect of cloud path.

uted to the increased travel distance for the cloud as it passed among the obstacles.

6.7 Summary—Concentration profiles through special obstacle arrays

The more pertinent observations with respect to cloud concentration are:

(i) the wind tunnel simulation of heavy gas dispersion in smooth terrain was representative of measurements made at full scale;

(ii) under the conditions simulated in this study, the presence of obstacles significantly affected heavy gas cloud dispersion, especially close to the release site;

(iii) further from the release point, the dispersion of heavy gas was not significantly affected by obstacles; and

(iv) at the highest windspeed tested (11 m/s), the presence of obstacles did not influence the dispersion of heavy gas more than the dispersion without obstacles.

7. Mathematical modelling of a heavy gas cloud spreading in still air

The mathematical modelling of a quasi-instantaneous release of heavy gas under calm or light wind conditions has been the subject of a number of studies (see [3], [4] and [11] for reviews of many of these approaches). The majority of these models separate the spread of a quasi-instantaneous release of a heavy gas into three phases: (1) the initial release phase, (2) the slumping phase, and (3) the passive phase. In the slumping phase, the gas cloud spreads primarily due to the density difference between the gas and the air. In the absence of strong external flow, this phase is dominated by buoyancy forces. This phase ends when the heavy gas is mixed with ambient air to the point where density differences between the cloud and ambient air are small.

In this study we focus solely on a portion of the slumping phase. Two methods have generally been employed in the mathematical description of the slumping phase: (1) finite difference models which solve the three-dimensional equations of motion for the cloud, and (2) box models in which variations within the cloud are integrated out and later may be re-incorporated through empirically determined profiles. In this study, the box model approach will be used to describe the horizontal cloud spread.

The box model approach used in this study assumes that the heavy gas is released as a cylindrical cloud of known dimensions [12]. The gas slumping phase of a heavy gas release is controlled by gravitational effects, resulting from greater gas density over that of the ambient air, and the shape of the advancing cloud. Thus, in this phase, the aerodynamic drag on the cloud ($\rho_a u^2 C_D A$) is balanced by the net hydrostatic pressure head ($hgA[\rho-\rho_a]$):

$$\rho_a u^2 C_D = hg\,(\rho-\rho_a), \tag{6}$$

where u is defined as either the frontal cloud speed or, alternately, the cloud spread rate; h is the depth of the cloud; C_D is the aerodynamic drag coefficient; ρ is the density of the heavy gas cloud; ρ_a is the density of air; and g is the gravitational acceleration constant. Equation (6) may be solved for u to give an expression of the form

$$u = C(ghd)^{1/2}, \tag{7}$$

where d is defined as the ratio of the density excess of the heavy gas over ambient air to the ambient air density, $(\rho\text{-}\rho_a)/\rho_a$, and C is a coefficient related to the drag coefficient and generally taken to be near unity [3,9].

Assuming a constant cloud volume ($V_0 = \pi hr^2$) during this phase and using the definition of velocity ($u = dr/dt$) results in the following relationship for the spread of the cloud under still air conditions:

$$r^2 = r_0^2 + 2Ct[gV_0 d/\pi]^{1/2}, \tag{8}$$

where r is the cloud radius at time t, r_0 is the initial cloud radius, and V_0 is the initial cloud volume. It should be noted that eqs. (6), (7) and (8) refer to cloud spread in an unobstructing terrain only, that is, one where the roughness elements are small compared with the depth of the cloud. These equations also assume no entrainment of ambient air into the heavy gas cloud (the constant volume assumption). Although this assumption has major impacts on the concentration time history (in effect, making concentration within the cloud constant through the slumping phase), it will be shown that entrainment of air into the cloud is not important in determining the cloud spread rate in a calm environment.

From the photographic records of the various release scenarios, we determined a value for C and the applicability of eq. (8) to cloud spread amongst a regular array of obstacles. These photographs were analyzed to determine the radial spread of the cloud at both the 90° (fastest spread) and 45° (slowest spread) angles from the horizontal corridor between the block sheets. From this analysis, a cloud radius versus time history was prepared for the seven scenarios. Note that the discussion of cloud movement in this study is limited to the model time frame from release to two seconds. At about two seconds after release, the cloud reached the limits of the study platform.

7.1 Comparison of experimental results with radial spread equation

Figure 29 shows the radius of the cloud plotted versus time for a flow direction along the unobstructed corridor (90°) under the full coverage scenario. Close examination of the data indicates that, for any given time, the radius of spread is generally least for the "no blocks" case and greatest for the 1:1 and 0.28:1 spacings with full coverage, a difference which increases with time. The radius of spread at a given time increases, therefore, as the area coverage of the blocks increases. With coverage of half the area by blocks ("half coverage"), systematic differences in the radii with respect to the "no blocks" case were not apparent (Fig. 30). It is evident, however, that the model (eq. 8) with

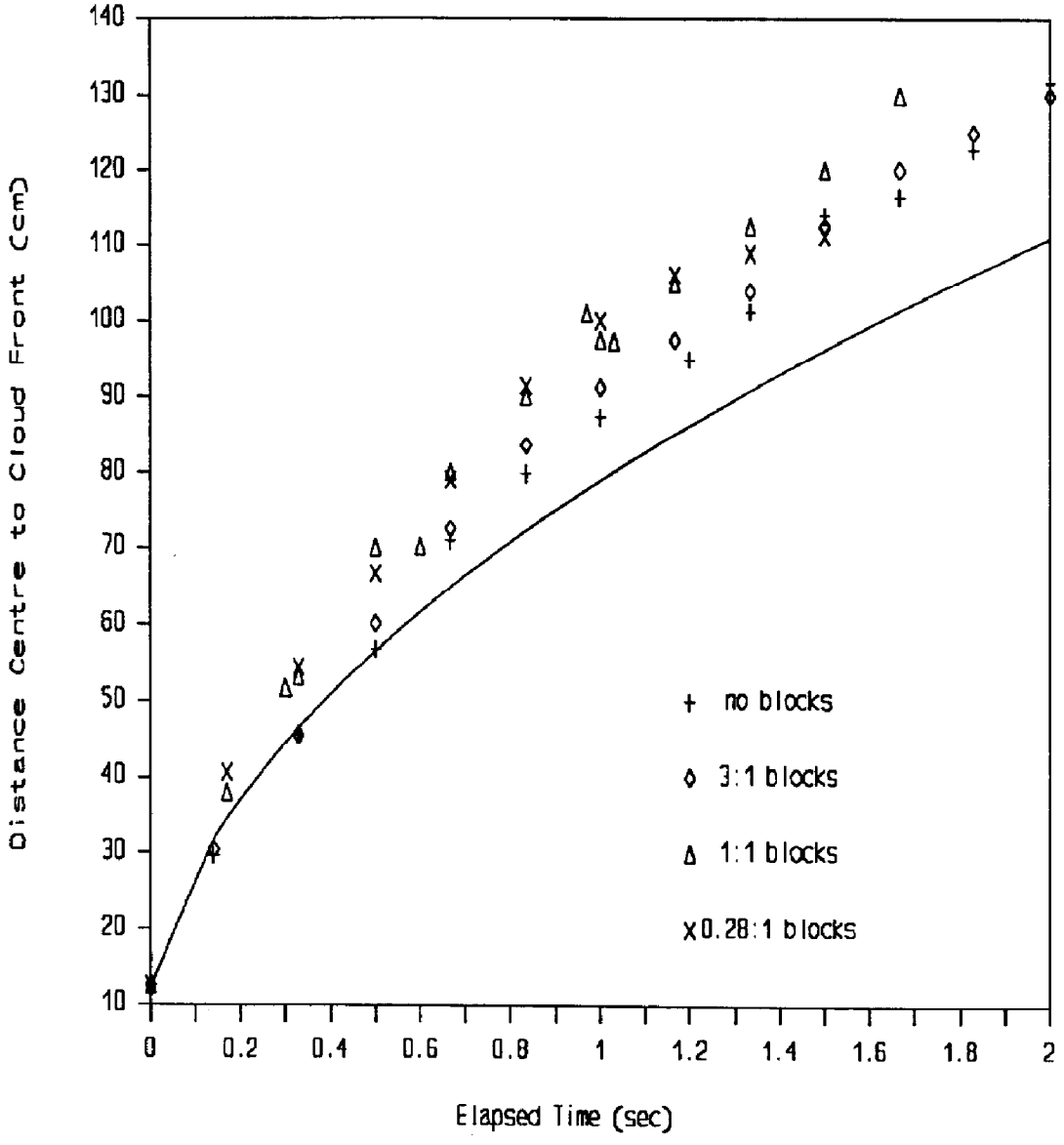

Fig. 29. Cloud spread at 90° angle to open corridor as a function of time for various block configurations—full block coverage.

$C=1$ (solid line in Figs. 29 and 30) is no longer a good fit to the measurements about 0.5 s after release.

Observations of the experimental releases show that the rate of cloud spread varied with the areal coverage of the blocks in the path of the gas cloud. Cloud movement for the full-coverage conditions down the obstruction-free corridors increase as the fraction of the area covered in blocks increases. Thus, for a given time, the cloud radius increases with coverage in the following sequence: no blocks, 3:1 coverage, 1:1 coverage and 0.28:1 coverage. In order to explain

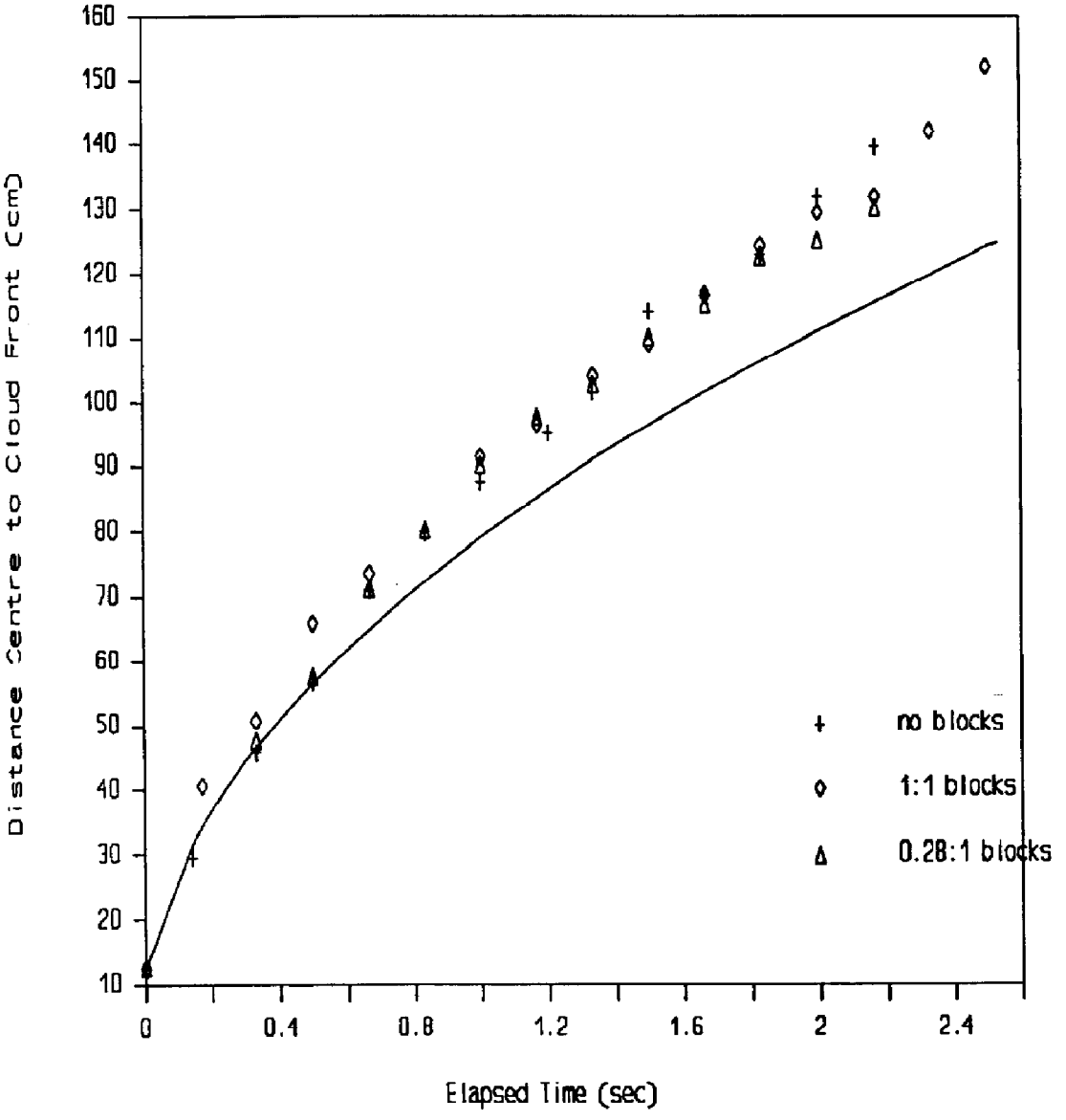

Fig. 30. Cloud spread at 90° angle to open corridor as a function of time for various block configurations—half block coverage.

the mechanism behind this behaviour, we recall that eq. (6) was derived from the balance of the frontal drag on the cloud and the net hydrostatic head exerted by the cloud. The hydrostatic head is a function of the depth of the cloud (h). Since we are assuming the volume of the cloud remains constant during this stage, the depth decreases as the radius increases. This assumption allowed us to derive eq. (8) from the balance of forces. However, in the case of flow through obstructions (i.e. the blocks), the shape of the cloud alters from the cylindrical. Regardless of the shape which the cloud takes, once it begins

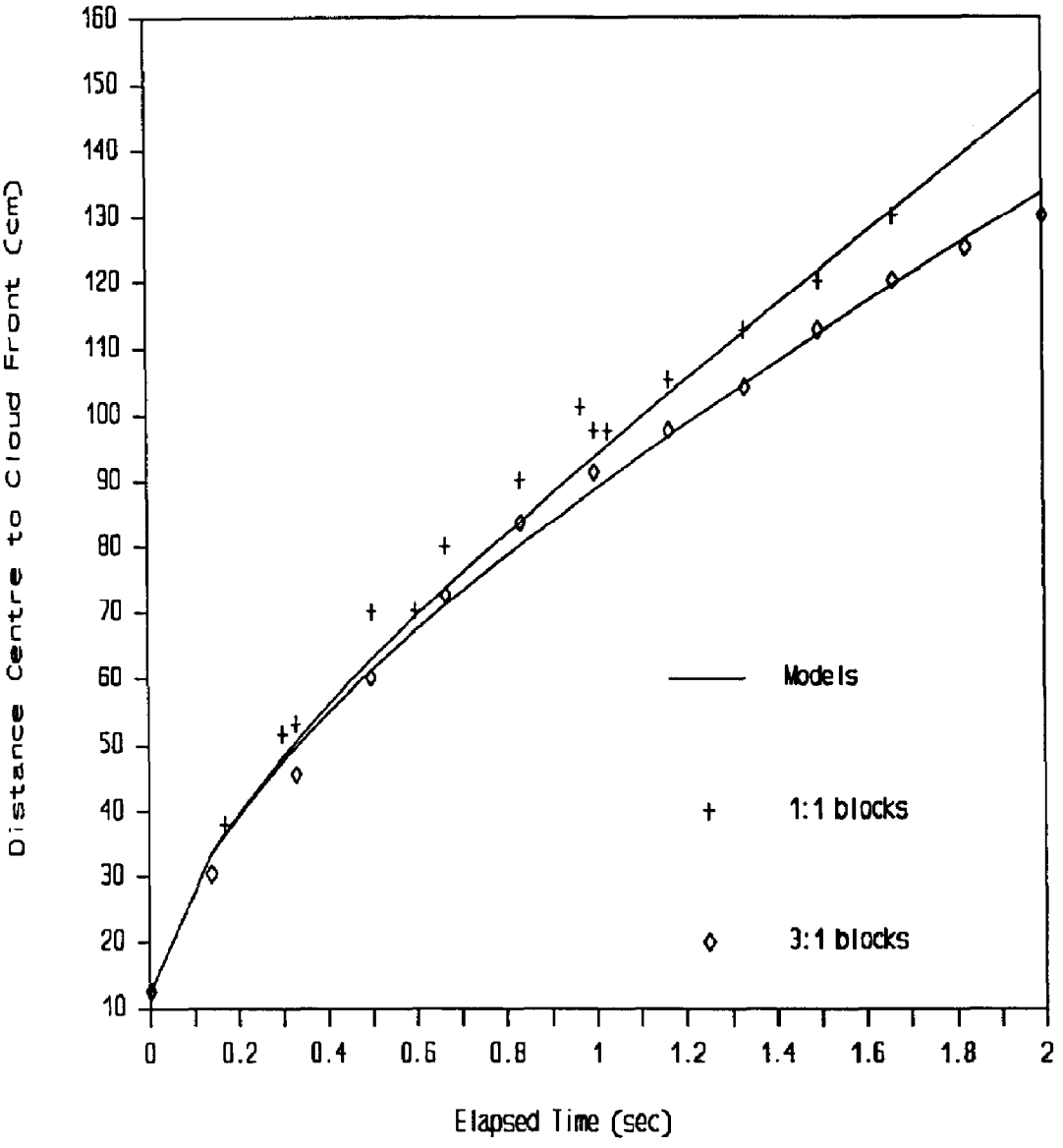

Fig. 31. Comparison between observed and modelled spreads for 1:1 and 3:1 block spacings—90° path.

to traverse the obstruction zone, the area of the ground surface covered by the cloud will be reduced. Assuming the obstacles are large in relation to the cloud depth, the reduction will be the difference between the area which would be covered if the cloud base was circular, with a radius equal to the most distant point of advancement, and the sum of the base areas of the blocks. If R_x is the most distant point from the center point of the cloud front, the potential area of surface coverage is πR_x^2. If the area covered by the obstructions is A_b, the actual area of the surface (A_{sc}) covered by the cloud is $\pi R_x^2 - A_b$. Since we are

TABLE 4

Model coefficients for various block configurations

Block configuration	A_c	γ	β
No blocks	0	0.11	0
3:1, Full coverage	0.06	0.14	0.13
1:1, Full coverage	0.25	0.25	0.60
1:1, Half coverage	n/a	0.13	0.60
0.28:1, Full coverage	0.60	0.45	5.0
0.28:1, Half coverage	n/a	0.12	5.0

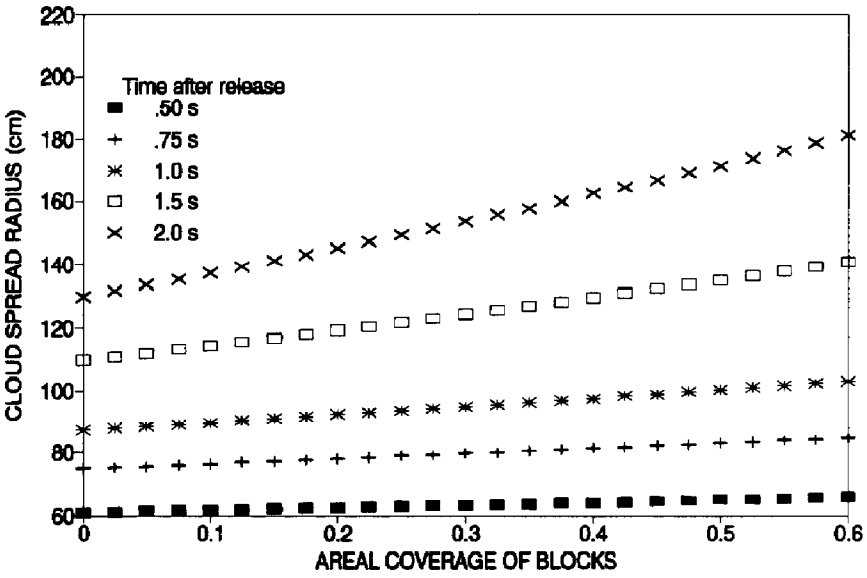

Fig. 32. Cloud radius versus obstacle areal coverage for several times after release.

still assuming constant volume, the depth of the cloud (h) is V_0/A_{sc}. From eq. (6) we may determine the cloud frontal speed down the corridor to be

$$u = \mathrm{d}r/\mathrm{d}t = (hCgd)^{1/2} = (V_0 Cgd/A_{sc})^{1/2}. \quad (9)$$

Thus, the rate of spread is an inverse function of the square root of the surface area covered by the cloud base which decreases as the block coverage increases. With no blocks, expression (9) reduces to (8). The integration of (9) results in a complex relationship which cannot be solved for r directly. Equation (8) can be forced to fit the experimental data through a portion of the spread with a change in the value of C (ranging from 1.19 to 1.75 [13]); however, the model using this range of values of C either underpredicted or overpredicted the cloud spread rate after about 1 s. Therefore, a relationship was sought which would unify the coefficients with a measure of block coverage and provide a better fit

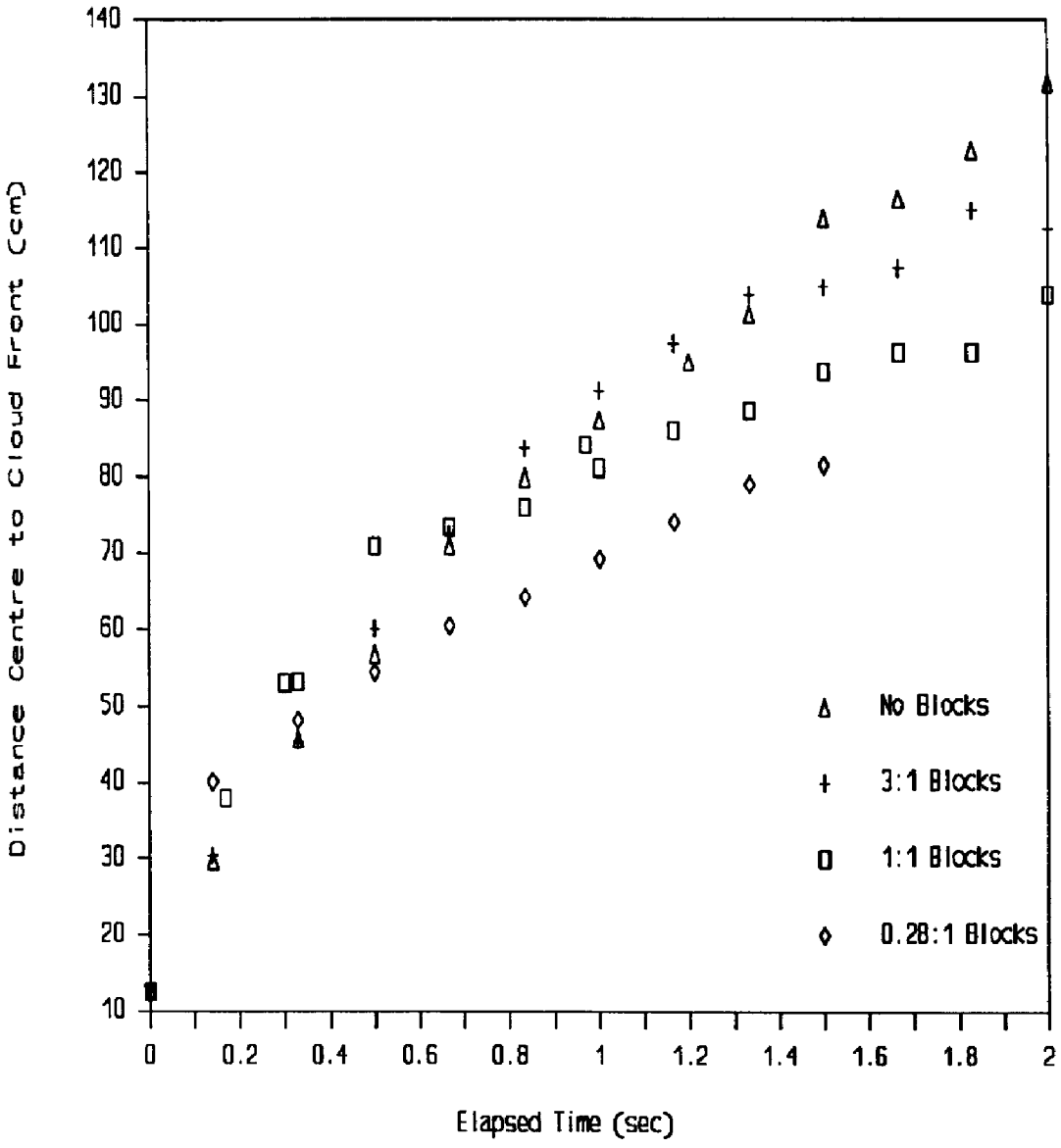

Fig. 33. Cloud spread at 45° angle to open corridor as a function of time for various block configurations—full block coverage.

to the observations over the two-second model time period. After some study, an empirical solution was determined in which C is replaced by C' exp (γt) where $C' = 1.1$ and γ is an empirically determined term which is a function of block coverage. Thus (8), the basic box model equation, becomes

$$r^2 = r_0^2 + 2C't[gV_0 d/\pi]^{1/2} \exp(\gamma t). \quad (10)$$

Note that eq. (10) indicates that the cloud will grow as t exp (t) which

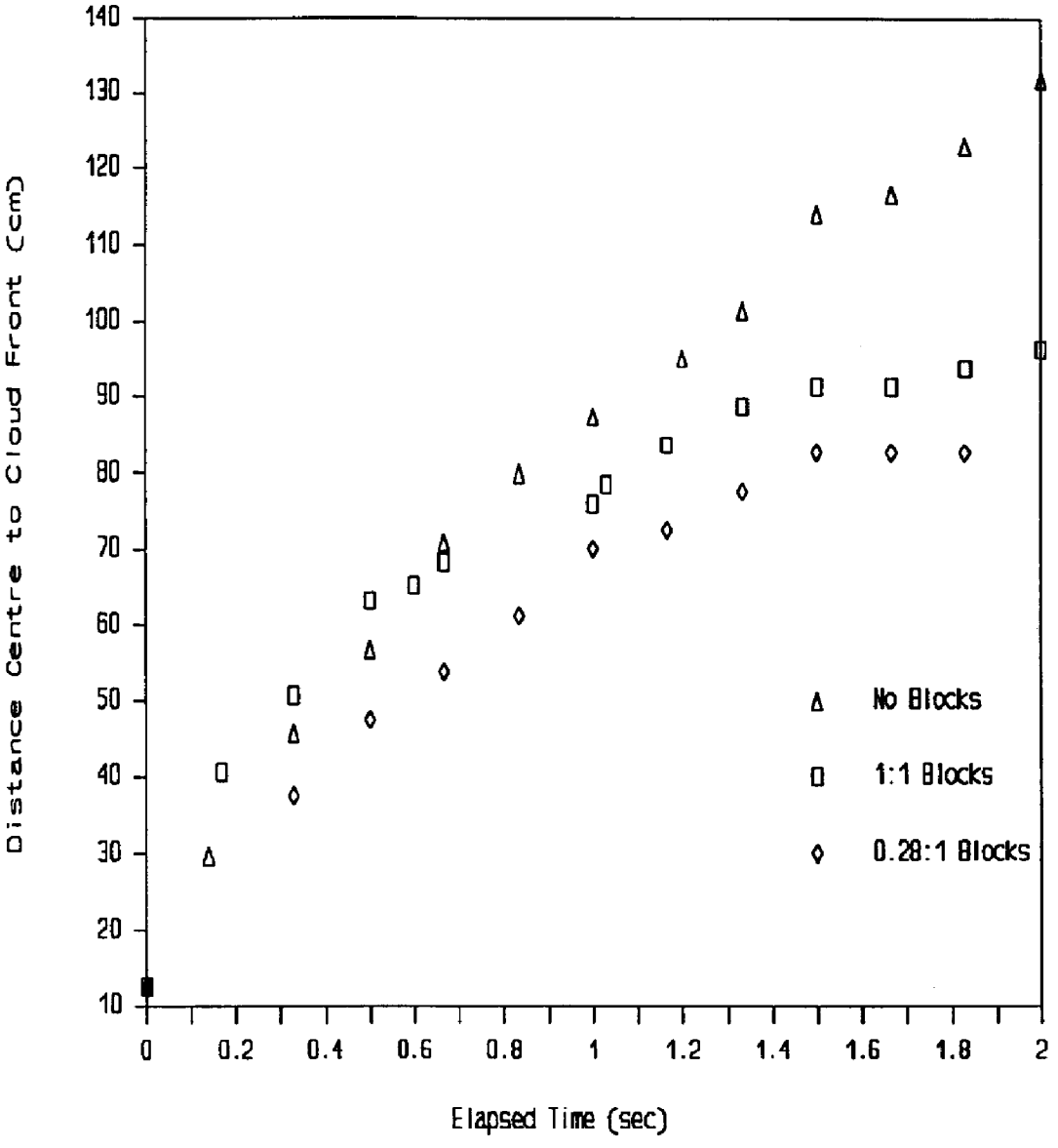

Fig. 34. Cloud spread at 45° angle to open corridor as a function time for various block configurations—half block coverage.

becomes large very rapidly. The slumping phase, however, is a finite phase of the heavy gas cloud lifetime and is expected to be short for most instantaneous cloud releases. In the experiments performed in this modelling study, the slumping phase is expected to last approximately 2–3 seconds after release. With this time restraint on (10), the cloud radius is of manageable size.

From the full coverage data, best-fit values of y were found to be linearly related to the fractional coverage of the blocks (A_c) as the percentage of block coverage varied from 0 to 60%. Based upon a linear regression fit to the data,

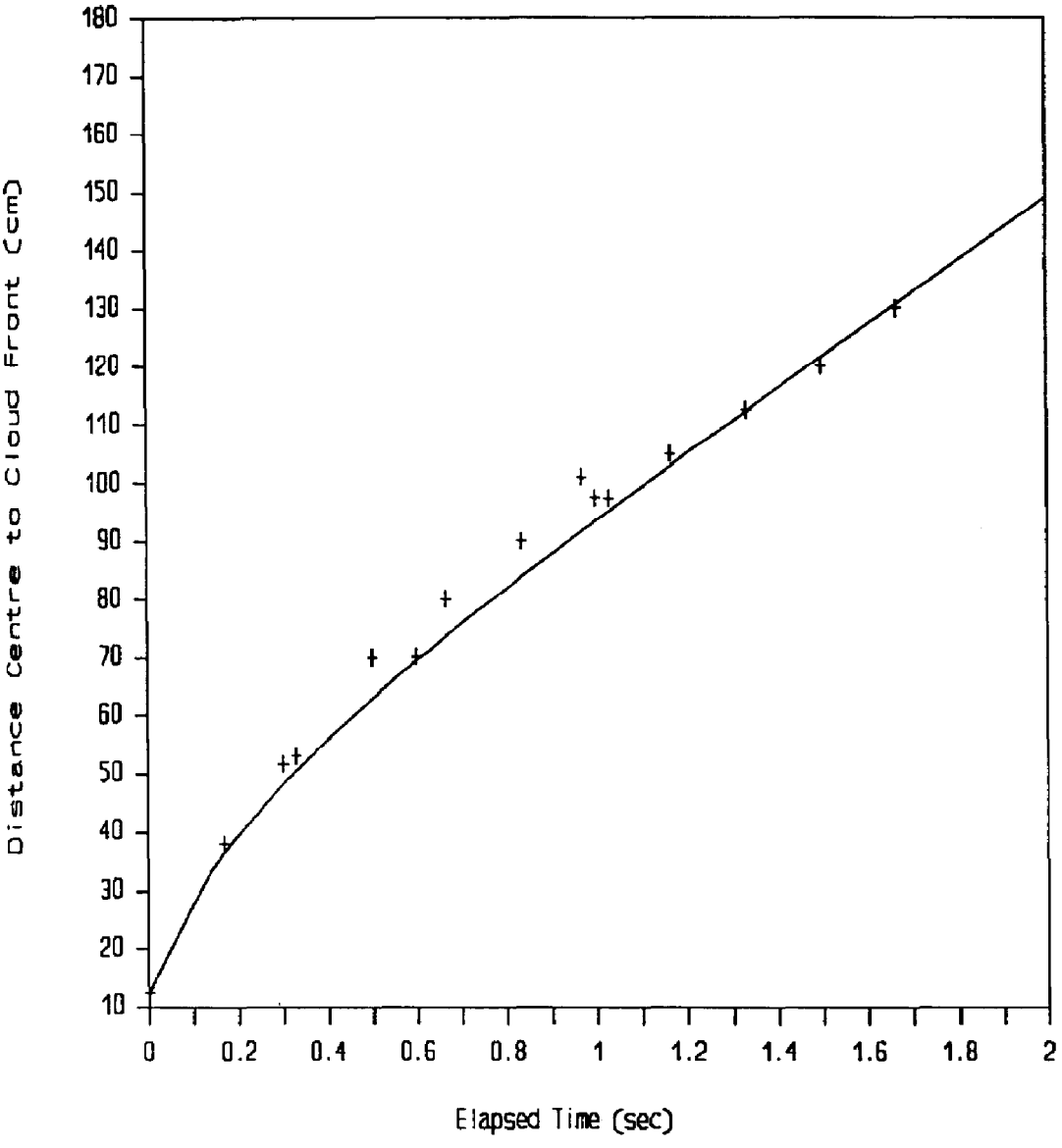

Fig. 35. Comparison between observed and modelled spreads for 1 : 1 full block coverage—45° path.

$\gamma = 0.11 + 0.56\ A_c$ where $A_c = s^2/(s+L)^2$, s is the length of the block and L is the separation of the blocks. With half coverage, however, γ, as determined by a best fit to the data, is approximately the same as for the "no blocks" case regardless of the degree of coverage on the blocked side.

Figure 31 shows the model expressed by eq. (10) plotted along with the experimental data for 3 : 1 and 1 : 1 block coverage. The comparisons of the model with the experimental data for each of the block configurations shows good agreement. Table 4 gives the values of γ for each block configuration.

The effect the γ-term has on the spread rate of the heavy gas cloud is greatest

for larger areal coverage and for longer times after release. Figure 32 shows the variation of cloud radius as a function of areal coverage coefficient for several times after release. It is evident from this figure that shortly after the release, the effect of the obstacles is minimal with respect to cloud radius—variations over a wide range of A_c are less than 20%—whereas for larger times the variation may be 50% or more.

For flow through the blocks, there is an inhibition of movement due to the presence of the blocks. Figures 33 and 34 show the distance of the cloud front as a function of time at an angle of 45° from the corridor for the various block configurations (full coverage and half coverage, respectively). Compared to the no blocks case, it is apparent from these data that, as the block spacing decreases, the cloud spread distance through the blocks also decreases.

An empirical relationship for the distance of spread through the blocks (r_d) from the time of release to about 2 s (model scale time) after release has been determined to be of the form:

$$r_d = rf(t,\alpha), \tag{11}$$

where r is the maximum radius of the gas cloud, and $f(t,\alpha)$ is a function of time and the angle α from the clear corridor (α ranges from 0° to 45°). The function $f(t,\alpha)$ may be expressed in the form

$$f(t,\alpha) = \{(\Phi - 1)\exp[-\beta t^2] + 1\}/\Phi, \tag{12}$$

where β varies with block coverage and $\Phi = (1+\tan\alpha)\cos\alpha$ specifies the path. With r expressed by (10) and $f(t,\alpha)$ by (12), a good fit between model prediction and experimental data may be obtained (for example, Fig. 35 for 1:1 spacing). Table 4 lists the best-fit values for b for each of the block configurations. For $\alpha = 0$ (flow down the corridor) or $\beta = 0$ (no blocks), $f(t,\alpha)$ equals 1 and r_d reduces to r. Therefore, the model expressed by the combination of eqs. (10), (11) and (12) is applicable for all flow situations for a regular block array.

Two experiments were also performed with the 1:100 canister with configurations of no blocks and 3:1 blocks—full coverage. For spread down the corridors, the radius of the cloud is defined by (10) with the $\gamma = 0.11$ for no blocks coverage. The measured values begin to diverge from the proposed model just prior to two seconds after release. Based on the flow visualization of these releases, it is believed that this divergence is due to the transition of the heavy gas cloud from the slumping phase to the passive phase. Britter [9] states that the expanding cloud vortex ring dissipates to the passive phases in a time of $40\text{–}60R_0/(dh_0)^{1/2}$ which for the small canister is 1.7–2.6 s, a range consistent with the model divergence from the measurements. Similarly divergence was not seen with the large (1:50) canister since the cloud leaves the study platform before this dissipation time (2.0–3.0 s after release) is reached.

8. Discussion of mathematical model for cloud movement

While the experiments upon which this analysis was based were limited to a short time span after release (<2 s real time), the work did encompass a large portion of the time in which the plume was expected to be in the slumping phase. Following Britter's estimate of the time at which a heavy gas cloud flow changes from the slumping phase to the passive phase [9], the change in character for the large canister would have occurred approximately 2-3 seconds after release. Limited experiments with the smaller canister indicated that the model predictions held throughout the slumping phase. Thus, the preceding analysis has shown that the spread of a heavy gas cloud released quasi-instantaneously into a calm environment can be adequately described by simple mathematical expressions derived from a balance of forces (eq. 6) for the first few seconds after release. Despite some simplifying assumptions, the fit between these simple spread models (eq. 9 and 10 and experimental release data is quite good. The following discussion comments on several of the simplifying assumptions.

In the development of the cloud spread equation (eq. 8), it was assumed that the cloud spread as a collapsing cylinder in which the volume remained constant. While the experiments performed both in this study (as discussed in Section 4) and in other field and wind tunnel tests ([3,10]) show that a cylinder of heavy gas released quasi-instantaneously spreads as a vortex ring rather than a cylinder, there is excellent agreement between the observed spread rate of the vortex ring and that expressed by equations such as (8).

Britter has commented that the agreement between the model expressed by (8) and observations should be considered fortuitous rather than an indication of the strict physical correctness of the model [9]. Indeed, the model assumes that the concentration within the cloud remains constant, an assumption which is contradicted by all observations which show substantial reductions in concentration as a result of entrainment of ambient air. Jensen [12], on the other hand, argues that the slumping velocity expressed by eq. (7) is independent of the amount of air entrained and is only dependent on the magnitude of the initial buoyancy of the cloud. The entrainment of ambient air is solely a function of the slumping velocity and exclusively increases the depth of the cloud.

In the calm situation, top entrainment of the heavy gas into the ambient air will alter the vertical concentration profile of the cloud from a "top hat" profile (constant concentration through cloud depth and zero concentration above) to one in which a layer of constant concentration is topped by a layer in which concentration falls from a maximum to zero in some fashion. It can be argued that, unless there is a loss of mass from the cloud (e.g. through deposition or advection), the pressure head caused by the heavy gas is the same for either vertical profile. With significant wind, however, the entrained upper portions of the cloud may be advected away from the main cloud body resulting in a loss

of mass and, therefore, a decrease in the hydrostatic pressure head. Such a process would, of course, alter the assumptions which allow us to derive (8) from (7).

It must be emphasized that the wind tunnel modelling experiments were designed to look at the bulk effects of obstacles which were large in comparison to the cloud height. The simulations were intended to model a large spill amongst a group of large obstacles such as might occur with a tanker truck or train car in an industrial park or urban area. It was not our intention to comment on smaller scale effects where the drag influence of the blocks on the local flow are definitely important nor on effects of surface roughness on cloud movement.

In the development of (9), it is hypothesized that, when obstacles are large compared with the cloud height, the bulk spread rate of a heavy gas cloud in calm air is affected more by the areal coverage of the blocks, through the maintenance of the hydrostatic pressure head, than through any effect on the aerodynamic drag on the cloud as expressed in the "constant" C. The proof offered is shown in the comparison of the full-coverage to the half-coverage results.

Looking at the flow rate through the blocks under a half-coverage scenario shows that the value of the parameter γ for best fit of (10) to the data (Table 4) is more similar to the no-blocks case than the corresponding full-coverage block configuration. It is argued that the lack of blocks on the upper half of the array increases the rate of reduction of the depth of the cloud and thus decreases the hydrostatic pressure head to values similar to those present in the no-blocks case. As a result, the cloud spread down the block corridor is the same as the radial spread in the blockless portion of the array. If the drag of the blocks was the dominant influence, the difference between the flow down the block corridor and in the block-free portion would be substantially different in the half-coverage case.

The cloud spread models expressed by eqs. (10) and (11) include terms which alter the model expressed by (8). These terms are, for the most part, empirical expressions of the effect of the block array placed in front of the cloud path. Equation (10), on first observation, is an attempt to flt a model to the data. On closer inspection, however, the term (11) may be considered as a term correcting (9) for the additional distance over which a parcel of gas moves through the blocks in a given time t after release. In the regular arrays considered, let us assume the rate of movement of the cloud front through the blocks is constant for a given block density. If the rate of movement (speed) is constant, then the distance the cloud front will travel for any given time after release will be the same for all parcels. Those parcels travelling down the unobstructed corridors will, of course, travel the furthest. Those required to find a path through the blocks will have a more circuitous route and therefore will travel a shorter radial distance from the canister.

This effect is readily observed in the comparison of the cloud spreads be-

tween the 1:1 block coverage with the regular array pattern and the 1:1 coverage with the staggered coverage. The only difference between these arrays is that for the staggered array every other row is offset by one block width. The effect of this stagger is that the open corridor which runs vertically for the regular 1:1 array is obstructed by blocks.

The diagrams shown in Fig. 9 are similar to those photographs taken in the flow visualization experiments for the 1:1 block spacing. Where blocks are far apart, such as in the 3:1 spacing, the path around the blocks is not greatly different from the clear corridors, and therefore the pattern is near circular. A similar pattern to Fig. 9(a) would develop for a number of regular patterns such as rectangular blocks with twice the width of the cubic blocks. It is proposed on intuitive grounds that, barring complete obstruction such as a wall, the pattern of a heavy gas cloud spread through obstacles will range between a square (diamond) and a circle. For a near-circular spread, the difference between the minimum and maximum radial spread distances will, of course, be minimal. For the square spread, this difference will be maximum. Thus, for a given areal coverage of obstacles (A_{sc}), the estimate of the maximum distance (x_{max}) for which a heavy gas cloud spreads in a calm environment may be determined from (10), and the minimum distance (x_{min}) may be determined from (10) using $\alpha = 45°$.

From the flow visualization experiments conducted in the wind tunnel, an empirical model has been developed which describes the spread of a heavy gas cloud in still air as a function of time during the early slumping phase of flow. The model equations are applicable to spread of the cloud across an area free of large obstacles as well as to flow through a regularly spaced field of obstacles which are large compared to the cloud. From the empirically determined coefficients in these equations, it is hypothesized that the major effect of the obstacles is to reduce the rate at which the hydrostatic pressure head declines rather than to retard the flow through friction or drag. The presence of the obstacles actually increases the rate of spread because of the slower decline in the pressure head. Flow among the blocks is perceived to be slower than flow down unobstructed corridors due to a longer travel distance required to circumvent the blocks, thus the term expressed by $f(t,\alpha)$ is only a function of obstacle and path geometry.

As a result of this study, refinements to the basic box model cloud spread equation (eq. 8) have been made. Although these new equations are based upon idealized obstacle arrays, they point toward a general equation for spread which includes a term dependent on the areal coverage of the obstacles (eq. 10). In an emergency response situation, this equation could be used to determine the minimal time required before a heavy gas cloud would reach a given point. For times shortly after release, the differences between cloud radii for a wide range of obstacle areal coverages is small, and eq. (8) is as good a predictor as eq. (10). However, for longer times the difference may be as great as 50%.

References

1 P.A. Irwin, M.C. Murphy, K.C. Heidorn and J. Xie, Scale Model Studies and the Development of Prediction Procedures for Heavy Gas Dispersion in Complex Terrain, MOE Contract Research Report No. 892014F, submitted to the Ontario Ministry of the Environment, Toronto, Ont., June, 1990.

2 R.N. Meroney, Wind tunnel experiments on dense gas dispersion, In: R.E. Britter and R.F. Griffiths (Eds.), Dense Gas Dispersion, Chemical Engineering Monographs, Vol. 16, Elsevier, Amsterdamm, 1982, pp. 85–106.

3 R.E. Britter and J. McQuaid, Workbook on the Dispersion of Dense Gases, HSE Contract Research Report No. 17/1988, Health and Safety Executive, Sheffield, 1988, 158pp.

4 S.R. Hanna and P.J. Drivas, Guidelines for Use of Vapour Cloud Dispersion Models, AIChE, Center for Chemical Process Safety, New York, NY, 1987, 177pp.

5 R.N. Meroney and D.E. Neff, Laboratory simulation of LNG vapour dispersion over land or water, Wind Eng., 2 (1980) 1139–1150.

6 R.N. Meroney and D.E. Neff, Physical modelling of 40 m^3 LNG Spills at China Lake, California, In: C. De Wispelaere (Ed.), Air Pollution Modelling and its Applications, New York, NY, 1981, pp. 449–462.

7 T.O. Spicer and J.A. Havens, Modelling the Phase I Thorney Island Experiments, In: J. McQuaid (Ed.), Heavy Gas Dispersion Trials at Thorney Island, Chemical Engineering Monographs, Vol. 22, Elsevier, Amsterdam, 1985, pp. 237–260.

8 J. McQuaid (Ed.), Heavy Gas Dispersion Trials at Thorney Island, Chemical Engineering Monographs, Vol. 22, Elsevier, Amsterdam, 1985, 435 pp.

9 R.E. Britter, Atmospheric dispersion of dense gases, Annu. Rev. Fluid Mech., 21 (1989) 317–344.

10 D.J. Hall and R.A. Waters, Comparison of Thorney Island results with wind tunnel-simulations, J. Hazardous Mater., 11 (1983) 209–236.

11 D.M. Webber, The Physics of Heavy Gas Cloud Dispersion, UKAEA Report, SRD R243, United Kingdom Atomic Energy Authority, Culcheth Warrington, 1983.

12 N.O. Jensen, On the Calculus of Heavy Gas Dispersion, Report RISØ-R-439, Risø National Laboratory, DK-4000 Roskilde (Denmark) 1981.

13 M.C. Murphy, K.C. Heidorn and P.A. Irwin, Scale model studies and development of prediction procedures for heavy gas dispersion in complex terrain 1988, Ontario MOE Technology Transfer Conference 1988, Toronto, Ont.